1 **Heterologous reporter expression in the planarian *Schmidtea mediterranea* through somatic**

2 **mRNA transfection**

3

4 Richard Nelson Hall[1,9], Uri Weill[2,9], Leonard Drees[2], Sergio Leal-Ortiz[3], Hongquan Li[4], Chew

5 Chai[1], Alejandro Sánchez Alvarado[5,6], Nicholas A. Melosh[3], Andrew Z. Fire[7,8], Jochen C.

6 Rink[2,*], Bo Wang[1,*]

7

8 [1]Department of Bioengineering, Stanford University, Stanford, CA, USA

9 [2]Department of Tissue Dynamics and Regeneration, Max Planck Institute for Multidisciplinary

10 Sciences, Göttingen, Germany

11 [3]Department of Materials Science and Engineering, Stanford University, Stanford, CA, USA

12 [4]Department of Electrical Engineering, Stanford University, Stanford, CA, USA

13 [5]Stowers Institute for Medical Research, Kansas City, MO, USA

14 [6]Howard Hughes Medical Institute, Kansas City, MO, USA.

15 [7]Department of Pathology, [8]Department of Genetics, Stanford University School of Medicine,

16 Stanford, CA, USA

17

18 [9]These authors contributed equally to this work.

19

20 *Correspondence should be addressed to J.C.R. (jochen.rink@mpinat.mpg.de) and B.W.

21 (wangbo@stanford.edu)

Abstract

Planarians have long been studied for their regenerative abilities. Moving forward, tools for ectopic expression of non-native proteins will be of substantial value. Using a luminescent reporter to overcome the strong autofluorescence background of planarian tissues, we demonstrate heterologous protein expression in planarian cells and live animals. Our approach is based on the introduction of mRNA through several nanotechnological and chemical transfection methods. We improve reporter expression by altering untranslated region (UTR) sequences and codon bias, facilitating measurement of expression kinetics both in isolated cells and in whole planarians using luminescence imaging. We also examine protein expression as a function of variations in the UTRs of delivered mRNA, demonstrating a framework to investigate gene regulation at the post-transcriptional level. Together, these advances expand the toolbox for the mechanistic analysis of planarian biology and establish a strong foundation for the development and expansion of transgenic techniques in this unique model system.

Keywords

Motivation

The study of planarians has contributed to advances in our understanding of regeneration, stem cell dynamics, and many other fundamental biological processes. However, the persistent challenge of expressing transgenes in planarians has led to the speculation that they may be resistant to transfection. In this work, we develop methods to express exogenous mRNAs in both isolated planarian cells and whole animals by optimizing delivery techniques, genetic constructs, and detection methods. These methods allow us to study transfection kinetics and post-transcriptional regulation of gene expression in a quantitative manner. Beyond planarian research, this work should also provide a broadly applicable strategy to develop similar tools for animals that are also challenging to modify genetically.

Introduction

Planarian flatworms have fascinated generations of scientists with their regenerative abilities and have played a critical role in our efforts to understand stem cells and regeneration (Newmark & Sánchez Alvarado, 2002; Reddien, 2018; Rink, 2018). Planarians can regenerate their entire body from a small tissue fragment. During this process, they restore their body axes and rebuild all organs to have appropriate proportions. While gene knockdown by RNA mediated genetic interference (RNAi) (Sánchez Alvarado & Newmark, 1999; Reddien et al., 2005; Collins et al., 2010) and next generation sequencing techniques (Böser et al., 2013; Lakshmanan et al., 2016; Guo et al., 2017; Grohme et al., 2018; Fincher et al., 2018; Plass et al. 2018; Guo et al., 2021) have been widely used in planarian research, tools for transgene expression are still needed. Earlier efforts have attempted whole animal electroporation of plasmid DNA encoding a fluorescence protein (González-Estévez et al., 2003), but the intense autofluorescence of planarian tissues and lack of orthogonal verification of transgene expression have limited the applicability of this study.

In general, establishing reporter expression in a system needs to overcome three challenges: construct delivery, expression, and detection. Delivery and expression are necessary prerequisites for detection, while, on the other hand, delivery and expression need reliable detection to optimize. In addition, strategies to circumvent various genetic defense mechanisms (Kim et al., 2019; Chen et al., 2003; Aljohani et al., 2020) that may restrict transgene expression are difficult to test without a robust reporter. Therefore, the first demonstration of reporter expression is often the bottleneck for developing transgenic tools; establishing a positive control can transform the method development process from a random walk in a vast parameter space into a well constrained optimization problem.

Injecting constructs into embryos often provides the first route for transgene expression in most systems. However, it is infeasible to inject in planarian's ectolethical eggs, as blastomeres are tiny and dispersed among yolk cells (Cardona et al., 2006; Davies et al., 2017). Furthermore, the commonly used planarian strains of *Schmidtea mediterranea* are exclusively asexual, reproducing through fission and regeneration (Benazzi et al., 1972; Vila-Farré & Rink, 2018). This leaves introduction of genetic material into individual somatic cells as the most general

81   approach to genetic modification in this system. While possible in some vertebrate models and

82   immortalized cell lines, transformation protocols and reagents are typically optimized for

83   specific systems. In addition, measuring delivery efficiency relies on expression as the ultimate

84   readout. Due to the distant relationship between planarians and other model organisms, it is

85   unclear what modifications to reporter constructs are needed to drive expression in planarians.

86   Finally, autofluorescence limits the utility of fluorescent proteins in planarians, especially during

87   the initial stages of reporter optimization when signals may be weak.

88

89   Here, we report a robust and extensively verified method for heterologous gene expression in

90   planarians. To address the problem of delivery, we used a direct nanoscale injection method to

91   first establish a positive control, based on which we identified efficacious chemical transfection

92   reagents for transforming planarian cells both *in vitro* and *in vivo*. To circumvent the numerous

93   variables associated with DNA transfections, we delivered synthetic mRNA for ectopic

94   expression. Finally, for detection, we relied on luminescent reporters, in particular, a compact,

95   bright, and stable luciferase, nanoluciferase, Nluc (Hall et al., 2012; England et al., 2016). Using

96   this sensitive and quantitative luminescence readout, we improved the reporter construct by

97   altering untranslated regions and codon usage biases and presented a case study in which we

98   identified regulatory sequences that modulate gene expression post-transcriptionally. Via

99   luminescence imaging, we quantified single-cell transfection kinetics and explored limiting

100   factors in transgene expression in planarian cells. Finally, we demonstrated the utility of

101   luminescence imaging for monitoring gene expression in live animals. Our results not only

102   provide the first positive control for exogenous gene expression in planarians to guide the future

103   development of planarian transgenesis, but also offer a new route to measure and understand

104   gene expression and regulation in planarian cells.

105

106   **Results**

107   *Nanoluciferase mRNA delivered through nanostraws is expressed in planarian cells*

108   To establish mRNA expression in the asexual strain of *S. mediterranea*, we sought to identify an

109   efficient platform for delivering genetic material into primary planarian cells. We selected

110   nanostraws, which combine the robustness of microinjection with the throughput of bulk

111   electroporation (Tay & Melosh, 2019).

4

112

113   Nanostraws are approximately 100-200 nm wide hollow aluminum oxide tubes protruding from

114   a polycarbonate substrate situated above a buffer reservoir containing the genetic material to be

115   delivered (**Figure 1A-B**). Cells are centrifuged against the straws which engage in close contact

116   with the cell membrane. Electric pulses are then used to locally porate the membranes and

117   electrophorese genetic material through the nanostraws and directly into the cellular cytoplasm

118   (**Figure S1**). By only permeabilizing membranes immediately in contact with nanostraws, they

119   have been shown to improve both delivery efficiency and viability of transformed cells (Xie et

120   al., 2013; Cao et al., 2018).

121

122   To prepare cells for nanostraw delivery, we flow-sorted a stem cell (i.e., neoblast) enriched

123   population based on their light scattering properties, so-called X1FS, from dissociated planarians

124   (Hayashi et al., 2006; Wagner et al., 2011). This population is uniform in size and depleted of

125   debris, which are important preconditions for nanostraw delivery. Our initial experiments used

126   capped and polyadenylated *in vitro* transcribed mRNA encoding the red fluorescent protein,

127   mScarlet, fused to the planarian histone H2B (**Table S1**). We reasoned that red fluorescence

128   might be more easily detectable against planarian autofluorescence (Lim et al., 2019), which is

129   biased towards shorter wavelengths, and that a nuclear localization signal might further enhance

130   signal-to-noise. We used a pulse train protocol that was empirically optimized for delivery in

131   human hematopoietic stem cells, which have similar morphological characteristics with XIFS

132   cells, i.e., small size, minimally adherent, high nucleus to cytoplasm ratio (Schmiderer et al.,

133   2020).

134

135   We performed flow cytometry to quantify fluorescence signal and found, even in this relatively

136   uniform cell population, a broad distribution of fluorescence intensities spanning three orders of

137   magnitude in both experimental and negative conditions (**Figure S2**), making the assessment of

138   transfection outcomes difficult. Since some cells genuinely exhibit brighter fluorescence than

139   others, false positives may be common and true positives could be obscured by the broad

140   autofluorescent background. These results compelled us to seek an alternative non-fluorescent

141   reporter to unambiguously quantify gene expression in planarian cells.

142

143   Unlike fluorophores, luciferases produce light as the result of an oxidative chemical reaction

144   with an exogenously added substrate (luciferin), and most animal tissues are devoid of

145   autoluminescence due to the enzymatic nature of luciferases (**Figure 1C**). Therefore, we

146   delivered mRNA encoding a planarian codon optimized nanoluciferase (sNluc1) (**Table S1**) into

147   X1FS cells. Transfected cells were maintained for 24 hr in Iso-L15, a nutrient rich medium with

148   reduced osmolarity. A similar medium has been shown to improve planarian cell viability (Lei et

149   al., 2019). We observed a clear and reproducible luminescence signal in transfected cells over

150   100-fold above the background signal of the negative controls. The physical dimensions of the

151   nanostraws strongly influenced the signal intensity, as has been observed in previous nanostraw

152   transfection experiments (Xie et al., 2013), implying that we were in a regime where expression

153   was dependent on the amount of mRNA delivered (**Figure 1D**). Overall, these results provide a

154   proof-of-principle for heterologous protein expression in planarian cells.

155

156   ***A screen identifies chemical reagents to efficiently transfect planarian cells***

157   With a validated reporter construct in hand, we next sought to identify a more broadly accessible

158   mRNA delivery method. Chemical transfection reagents have become increasingly popular

159   because of their ease of use, high efficiency, and scalability, but they are often developed and

160   optimized for specific cell types.

161

162   To identify suitable reagents for planarian cell transfection, we screened a panel of commercially

163   available reagents by transfecting *in vitro* transcribed sNluc1 mRNA containing 5' and 3' UTR

164   sequences from a highly expressed planarian gene, Y-box binding protein (*YB1*) (**Table S1**), and

165   measuring the luminescence on a plate reader. Our screen used total cells from freshly

166   dissociated animals rather than X1FS cells due to the large number of transfections needed

167   (**Figure 2A**). Initially, all reagents were utilized according to the manufacturer's recommended

168   protocols (**Table S2**). While most transfection reagents produced little to no expression, Viromer

169   and Mirus Trans-IT reagents, both of which are comprised of endoosmolytic cationic polymers,

170   consistently achieved luminescent signals 100 to 1,000-fold above the negative control (**Figure**

171   **2B**).

172

6

173   To further optimize the transfection protocols, we tested various ratios between Nluc mRNA and

174   reagent components (**Figure 2C-D**). For Viromer, increasing both the amount of reagent and/or

175   mRNA in the transfection mix doubled the baseline signal, with 0.8 µL of reagent per 1 µg

176   mRNA per reaction as an economic compromise for further experiments. A similar two-fold

177   boost over the baseline signal was achieved for Trans-IT, but maximal signal intensities in cell

178   cultures remained below those achieved by Viromer transfections. These conditions, however,

179   still only produced luminescence ~100-fold lower compared to transfections of mammalian cells

180   (e.g., HeLa cells) (**Figure S3**), indicating that future optimizations might help to achieve

181   substantially higher expression levels.

182

183   To confirm that luminescence was produced by transfected planarian cells, we imaged cells

184   transfected with nanostraws, Trans-IT, and Viromer using NanoGlo-Live furimazine substrate

185   (Promega) on an LV200 bioluminescence imaging system (Olympus). Individual luminescent

186   cells were evident in transfected samples (**Figure S4**) but never observed in negative controls.

187   High magnification imaging confirmed the cytoplasmic origin of the luminescence signal. By

188   counting luminescent live cells over time, we quantified the transfection efficiency to be ~3.5%

189   out of all cells for Viromer, which plateaued starting ~12 hr post transfection (hpt), and 0.2% for

190   Trans-IT (**Figure 2E**), whereas cell viability was similar after both transfections (**Figure 2F**).

191   Comparing both reagents, the discrepancy in percentage of luminescent cells is smaller than the

192   difference in total luminescence intensity measured by the plate reader, suggesting that Viromer

193   transfected more cells and produced higher expression per cell. Finally, to further demonstrate

194   that Nluc mRNA is the source of the luminescence, we created a Nluc variant containing a

195   premature stop codon, which completely abolished expression and thus provided additional

196   evidence for transgene expression in planarian cells (**Figure S5**). Overall, these observations

197   establish chemical delivery as a viable method for mRNA transfection of planarian cells, with

198   Viromer and Trans-IT as promising leads.

199

200   ***Altering untranslated region (UTR) sequences and codon bias improves Nluc expression***

201   With efficient delivery reagents, we sought to improve the reporter construct. To identify UTRs

202   that may enhance expression, we flanked sNluc1 with UTRs (**Figure S6-7**) from four

203   endogenous genes with high expression in all cell types, reasoning that they may enhance Nluc

204   mRNA stability and/or translation efficiency (see **Table S3** for sequence details). These UTRs

205   either increased (RPL15, YB1, RPL10) or decreased (ENO) the expression of Nluc relative to

206   the construct lacking endogenous UTRs (**Figure 3A**).

207

208   Next, we investigated the effect of codon optimization, the commonplace practice of matching

209   endogenous codon biases in order to maximize expression (Quax et al., 2015; Jeacock et al.,

210   2018). This may be important for *S. mediterranea*, in which a strong preference for A/T at third-

211   base positions contributes to a genome-wide A/T-bias of 70% (Grohme et al., 2018). Therefore,

212   we generated five additional codon-optimized Nluc variants, besides sNluc1, to cover a range of

213   codon adaptation indices (CAI), a 0-1 bounded value measuring the gene's codon bias compared

214   to a reference codon preference table (Sharp & Li, 1987; Puigbò et al., 2008). We also included a

215   Nluc sequence optimized for mammalian expression (hNluc) as a comparison. Unexpectedly, the

216   luminescence in transfected cells did not correlate with CAI (**Figure 3B**). The most highly

217   expressed construct (sNluc2, CAI = 0.713) was part of a series of constructs with very similar

218   CAIs and GC content generated by randomly sampling the planarian codon table (sNluc2-4;

219   **Tables S1, S3**). Based on these results, we combined RPL15 UTR and sNluc2 into an improved

220   reporter construct that was used for all subsequent experiments unless otherwise explicitly

221   specified (**Figure S8**).

222

223   *Live luminescence imaging reveals expression kinetics in vitro*

224   Quantifying expression levels across cells and changes within single cells can help reveal

225   important kinetics of transfection and gene expression. For quantitative microscopy, we built a

226   customized luminescence microscope (Kim et al., 2017). Using a demagnifying tube lens, we

227   expanded the field-of-view (FOV) of high magnification/high numerical aperture (NA)

228   objectives that are needed for efficient light collection. In addition, we used a back-illuminated

229   EMCCD camera (Andor iXon) for detection, which has single-photon sensitivity and provides

230   quantitative measurements. The conventional substrate for Nluc, furimazine (Fz), has poor water

231   solubility and is supplied in organic solvents which may stress cells and affect gene expression

232   kinetics. To overcome this, we utilized a novel Fz derivative, fluorofurimazine (FFz), which has

233   improved water solubility and thereby reduces cytotoxicity while maintaining Nluc's

234   characteristic brightness (Su et al., 2020).

235

236   With these technical advances, we quantified the distribution of luminescence intensities across

237   transfected cells. For this experiment, bulk dissociated cells were allowed to adhere to a glass-

238   bottom imaging well treated with concanavalin A to prevent them from moving in and out of the

239   imaging plane. We first imaged cells at 24 hpt, as at this time point the number of luminescent

240   cells should have plateaued (**Figure 2E**). In a single FOV (~1.6 mm^2), we captured over 80

241   individual luminescing cells (**Figure 4A**). From these images, we segmented cells and quantified

242   their luminescence at 40 min post FFz addition, to allow sufficient time for FFz to diffuse into

243   the cells. This revealed a long-tailed distribution with a small number of intensely bright cells

244   (**Figure 4B**). Unexpectedly, we captured new transfection events even at this late time point,

245   indicating that not only were these cells healthy enough to be transfected, but also that there

246   remained functional Viromer-mRNA complexes in the media (**Figure 4C**).

247

248   Motivated by the observation that we could capture individual transfection events, we performed

249   imaging from the moment of transfection to measure the kinetics of transfection and the onset of

250   expression. We added transfection complexes and FFz at the same time and immediately began

251   imaging. The sample started completely dark, but within the first hour many cells began to

252   luminesce (**Figure 4D**, **Video S1**). We quantified the luminescence of each cell (**Figure 4E**) and

253   extracted the transfection time, defined by the time when the luminescence exceeds the

254   background noise. The transfection time followed a gamma distribution (**Figure 4F**), suggesting

255   that transfections are independent stochastic events, though the rate of transfection likely varies

256   over time. The mean transfection time was ~140 min post transfection (mpt), with events

257   scattered throughout the time we imaged. This time scale is consistent with the fast kinetics of

258   mRNA transfection and translation (Leonhardt et al., 2014). Most cells reached their maximal

259   luminescence rapidly post transfection, whereas a few cells grew luminescent over a longer

260   period (**Figure 4G**). To quantify the rate of translation, we measured the difference between the

261   time when luminescence maximizes (t_{max}) and the time at which transfection occurs (t_0) and

262   found that on average cells reached their maximum luminescence within 60 min after

263   transfection (**Figure 4H**).

264

265   Over time, we noticed that the luminescence in individual cells never plateaued but instead

266   became dimmer after the peak over the course of a few hours regardless of the transfection time

267   (**Figure 4E**, **Video S2**). This phenomenon is unexpected as even if mRNA, once delivered, is

268   rapidly degraded within the cytoplasm, Nluc protein is reported to have a half-life of ~8 days in

269   cell lysates (Hall et al., 2012). In addition, Nluc is an ATP-independent luciferase, and therefore

270   should not depend on cell metabolism to luminesce. We wondered whether the dimming was

271   primarily due to substrate depletion, so we added additional substrate after the first imaging

272   session when only a few dimly luminescent cells remained. While some cells indeed recovered

273   partially, most cells remained dark (**Figure S9**), suggesting that substrate availability was not the

274   limiting factor. Notably, we occasionally saw cells burst open, releasing Nluc into the media.

275   This was evident from the single-cell luminescence showing a sudden spike and an immediate

276   drop at the moment of rupture (**Figure 4I**). However, these events were rare during our imaging

277   experiments, so cell death was not the major cause of luminescence decay either. These results

278   implied that either planarian cells have special mechanisms that caused Nluc to be particularly

279   unstable or sequestered, or Nluc was released, actively via secretion or passively through leaky

280   membranes, though the exact mechanism requires further investigation. Together, these results

281   suggest that it is feasible to image Nluc in live cells at high temporal resolution, which provides a

282   powerful tool for quantifying gene expression kinetics in planarian cells.

283

284   *mRNA transfection can reveal post-transcriptional regulatory elements*

285   The ability to transfect and express exogenous mRNA also opens new possibilities for the

286   analysis of gene regulation in planarians, which have so far been limited to observing phenotypic

287   and measuring genotypic changes under the influence of RNAi. For example, the synthesis of an

288   mRNA and the abundance of its encoded protein can be decoupled by cis-acting elements in the

289   5' and 3' UTRs that affect translation or mRNA stability. Understanding which regions of a UTR

290   sequence are responsible for such post-transcriptional regulation requires the ability to remove or

291   add putative regulatory elements to a reporter gene and study how its expression is altered.

292

293   As a case study, we selected a transcript (dd_Smed_v6_62_0_1) which contains two long

294   overlapping open reading frames (ORF1: 513 nt, ORF2: 483 nt) with ORF1 beginning 40 nt

295   upstream of ORF2. To resolve which ORF (or both) is translated, we created two constructs with

10

296   Nluc beginning at the start codon of each reading frame. Transfecting these reporters into bulk

297   dissociated cells showed that the translation was specific to the first open reading frame (ORF1),

298   as Nluc expression was barely detectable from the ORF2 (**Figure 5A**). Removing the start codon

299   of ORF1 by replacing the 5' UTR with a synthetic sequence (attP1) recovered the Nluc

300   expression. Thus, translation of these transfected RNAs was consistently initiated from the

301   upstream start codon.

302

303   Next, we investigated the function of the 3' UTR. For this, we successively truncated the 3' UTR

304   from the ORF1 Nluc construct. We found that removing the end of the 3' UTR, nucleotides 141-

305   188 (Δ47), increased the expression by 3-fold, suggesting the presence of a destabilizing or

306   repressing element within this region; deleting additional sequences had minimal additional effects

307   (**Figure 5B**). Surprisingly, adding a short synthetic sequence (M13R) to the 3' end of the full-

308   length UTR drove considerably stronger expression (**Figure 5A**), implying that the function of the

309   putative repressive or destabilizing elements may be sensitive to sequence context. Overall, these

310   results provide a platform for studying post-transcriptional regulation in planarian cells.

311

312   *Heterologous reporter expression in live animals*

313   Although the ability to transfect planarian cells with mRNA *in vitro* represents a significant

314   advance in the genetic manipulation of planarian cells, current planarian cell culture is limited by

315   low cell viability, lack of cell proliferation, and the gradual loss of neoblast identity (Kai et al.,

316   2019), thus limiting the range of questions that can be addressed in isolated cells. We therefore

317   explored whether our transfection protocols might be sufficient for generating reporter

318   expression in whole animals.

319

320   We injected RPL15-sNluc2 mRNA complexed with Viromer or Trans-IT into the parenchymal

321   tissue along the tail midline, which reduces the risk of misinjections into the abundant gut

322   branches (**Figure 6A**). We then measured bulk luminescence on individually dissociated worms

323   at multiple time points post transfection. The luminescence background in tissue lysates from

324   sham-injected animals was universally very low, mirroring what was observed *in vitro*. In

325   contrast, mRNA injection with Viromer or Trans-IT led to luminescence signals up to 1000-fold

326   above background (**Figure 6B-C**). For Viromer, the highest fraction of expressing animals was

11

327   detected already at 2 hpt (30/30) and remained robust for 12 hpt (29/30) (**Figure 6B**). Contrary

328   to our observations *in vitro*, Trans-IT transfections produced luminescence intensities stronger

329   than those of Viromer transfections by an order of magnitude (**Figure 6C**), suggesting that for *in*

330   *vivo* transfections, Trans-IT is more effective than Viromer.

331

332   To confirm that luminescence came from cells, we dissociated transfected tails, and through

333   imaging, we observed high densities of luminescent cells (**Figure S10**). Further, we succeeded in

334   validating Nluc expression using Western blotting. Initial efforts using an anti-Nluc antibody

335   failed due to poor binding characteristics; as a result, we transfected planarians with RPL15-

336   sNluc2 flanked by two 3× FLAG affinity tags. Western blotting against anti-FLAG produced a

337   clear band, providing an orthogonal validation of Nluc expression (**Figure 6D**). As a

338   comparison, an equivalent mass of transfected HeLa cell lysate was also blotted, which produced

339   a significantly brighter signal consistent with the higher expression observed in luminescence

340   assays. Together, these results establish mRNA reporter delivery and expression in live

341   planarians.

342

343   We next asked whether Nluc expression was sufficient for luminescence imaging *in vivo*. We

344   injected at either the tail midline or behind the left eye and incubated the animals for 15 min in

345   NanoGlo-Live substrate supplemented with 1% DMSO to aid in tissue penetration. The

346   immobilized animals were then imaged on an LV200 (Olympus) microscope. This experiment

347   revealed bright luminescence after both Viromer and Trans-IT injections, while no luminescence

348   was detected in negative controls injected with mRNA alone (**Figure S11**). Although the spatial

349   resolution of *in vivo* luminescence imaging did not allow for cellular resolution, the small size of

350   the luminescent region was consistent with the transfection of a small cluster of cells around the

351   injection site.

352

353   Luminescent reporters are particularly attractive for live imaging of planarians, as these animals

354   are photophobic and become agitated by the intense excitation illuminations required for

355   fluorescence experiments. Therefore, we tested time-lapse imaging of unrestrained animals and

356   succeeded in tracking luminescent patches between frames (**Figure 6E**, **Video S3**). For these

357   experiments, we used FFz as a low toxicity substrate and found that the animals can be recovered

12

358   alive after a few hours of imaging. Encouraged by this result, we then imaged planarians right

359   after injecting Trans-IT-mRNA complexes to determine expression kinetics *in vivo.* We further

360   increased the luminescence signal by injecting the FFz substrate directly into the planarian gut to

361   improve the bioavailability and to reduce the amount of FFz used per experiment. By

362   continuously imaging for ~1 hr, we observed similarly rapid expression kinetics consistent with

363   our observations *in vitro* (**Figure 6F-G**, **Video S4**). These results represent the first direct

364   measurement of gene expression kinetics in a live planarian, which establishes luminescence as a

365   route for quantitative live imaging through thick, strongly autofluorescent tissues.

366

367   **Discussion**

368   Transgene expression in planarian flatworms has been a persistent challenge in the field since the

369   molecular biology revival of the system around two decades ago (Agata & Watanabe, 1999;

370   Newmark & Sánchez Alvarado, 2002). Here, we accomplished heterologous protein expression

371   in the planarian model species *S. mediterranea* by combining four experimental approaches: (1)

372   nanostraw electro-delivery to establish an initial positive control, which enabled subsequent

373   optimization of chemical delivery methods; (2) delivering mRNA instead of DNA to bypass the

374   complexities of nuclear import, transcription, and splicing; (3) optimizing post-transcriptional

375   factors to enhance expression; and (4) using a luminescent reporter to circumvent the strong

376   autofluorescence which complicates the use of fluorescent reporters. By making these choices,

377   we observed a clear signal from exogenously supplied Nluc mRNAs in planarian cells both *in*

378   *vitro* and *in vivo*.

379

380   Exogenous reporter expression in our results is supported by multiple independent lines of

381   evidence. First, we showed that planarians are minimally autoluminescent, and most

382   experimental conditions tested reproducibly reached luminescence intensities as high as 3-4

383   orders of magnitude above the background, which makes the detection of false positives

384   extremely unlikely. Second, we observed that luminescence showed a dose-dependence on Nluc

385   mRNA amounts, which was abolished by the addition of a premature stop codon. Third,

386   luminescence intensity was modulated by biologically relevant factors such as UTR sequences

387   and codon usage bias. Fourth, imaging of transfected cell cultures confirmed a cytoplasmic

388   origin of the luminescence signal, and time-lapse imaging showed rapid expression kinetics in

389   single cells consistent with mRNA expression. Fifth, we succeeded in imaging luminescence in

390   live injected animals, with the signal consistently restricted to the injection site. Sixth, we were

391   able to detect Nluc protein via Western blotting from tissue lysates of transfected animals.

392   Finally, the results presented in this manuscript were gathered in two different laboratories,

393   which highlights the robustness and general applicability of the technique. Collectively, our

394   results represent the first unambiguous demonstration of exogenous mRNA expression in

395   planarians.

396

397   In terms of direct utility, our current reporter assay represents a significant expansion of the

398   planarian toolkit. We demonstrated that by delivering Nluc mRNA, we were able to identify

399   successful transfection methods and subsequently optimize them. New gene delivery strategies

400   are being developed at a rapid pace, including dendrimers, nanoparticles, virus-like particles

401   (VLPs), and cell-penetrating peptides (Lostalé-Seijo & Montenegro, 2018). Our methodology

402   can be continuously applied to screen this ever-expanding repertoire of transfection techniques to

403   achieve more efficient delivery, lower cytotoxicity, and higher expression. Similarly, this

404   approach can be used to assess other mRNA-based expression systems such as self-replicating

405   RNA replicons including alphavirus (Beal et al., 2015) and nodamuravirus (Taning et al., 2018),

406   which may help to overcome mRNA's transient expression and increase overall luminescence

407   intensity. In even broader contexts, our method also allows testing additional reporters and

408   transfecting other species, with initial success reported in **Figure S12** and **Figure S13**,

409   respectively.

410

411   Importantly, the use of FFz, a novel water-soluble furimazine derivative, allowed us to monitor

412   the kinetics of transfection and expression *in vitro* and *in vivo* by time-lapse luminescence

413   imaging. This technique could be used not only to assess novel transfection reagents for

414   favorable kinetics, but also to monitor the dynamics of biologically relevant processes occurring

415   on the timescale of minutes to hours. Luminescent reporters have two clear advantages over

416   fluorescent reporters for live imaging applications. First, planarians are photophobic and escape

417   quickly from the bright excitation lights used in fluorescence imaging. Second, planarians are

418   highly autofluorescent, which makes interpreting weak fluorescence signal difficult if not

419   impossible. With luminescence, we detected Nluc expression in unrestrained animals and

14

420   captured initial expression kinetics on live animals immediately after transfection. We anticipate

421   that the ability to sensitively detect Nluc expression *in vivo* will be valuable for screening other

422   expression systems, such as DNA-based transgenesis, especially since animals may be recovered

423   alive after luminescence imaging.

424

425   Beyond the technical applications, we demonstrated that Nluc mRNA transfections can be used

426   to study post-transcriptional regulation, a biological application that we anticipate will be of

427   broad interest. In particular, we quantitatively measured the consequences of varying UTR

428   sequences. This approach provides a route to identify novel cis-regulatory sequences, which

429   would be impossible otherwise. Such sequences may serve as tools for further controlling gene

430   expression through a broader dynamic range. Besides UTRs, our method allows for exploring

431   other post-transcriptional regulatory mechanisms in planarians, such as incorporating trans-

432   spliced 5' leader sequences (Zayas et al., 2005; Rossi et al., 2014), adding target sites of known

433   small RNAs (Kim et al., 2019), including internal ribosomal entry sites (IRES), or manipulating

434   secondary structures of mRNA (Leppek et al., 2022). Our study sets the stage for the systematic

435   characterization and analysis of these factors to better predict how sequence informs expression.

436   In addition to regulatory sequences, the individual nucleotides in mRNA can be modified to

437   increase RNA expression and/or stability (Andries et al., 2015; Svitkin et al., 2017). As a first

438   attempt, we synthesized mRNA incorporating the canonical uridine versus mRNA containing the

439   base analog 1-methyl pseudouridine (m1Ψ) and found that both RNAs were capable of

440   expression in planarians. While we did not observe any significant differences in expression

441   levels (**Figure S14**), our method provides a route to explore the effects of other modified

442   nucleotides on mRNA expression in planarian cells.

443

444   Achieving planarian transgenesis will require solving numerous challenges, including gene

445   delivery, expression, and detection. Our method addresses them by utilizing several transfection

446   reagents to deliver a Nluc reporter construct, the expression of which we can unambiguously

447   detect and quantitatively measure. Collectively, these narrow the enormous parameter space that

448   makes the *de novo* establishment of transgenesis in phylogenetically distant model systems so

449   challenging. As such, our results transform the quest for planarian transgenesis from a trial-and-

450   error process into a constrained parameter optimization process, which we anticipate proceeding

15

451 rapidly with our community. More broadly, we predict that our strategies may also prove useful

452 for manipulating other asexually reproducing animals which lack a germline and cannot

453 otherwise be transformed through embryonic manipulations.

454

455 **Limitations of Study**

456 Compared to the current state of the art in established genetic model systems, the absolute level

457 of reporter expression is relatively low in our study. Although this limits the use of fluorescent

458 reporters (especially given the strong autofluorescence of planarian tissues), we found that Nluc

459 enabled the development of a much higher signal-to-noise reporter, allowing sensitive and

460 quantitative detection of gene expression, especially when used with improved water-soluble

461 substrates. In addition, the chemical transfection reagents were screened and optimized on total

462 cells, which may limit their efficacy and specificity on stem cells (neoblasts). While we detected

463 Nluc expression in neoblast-enriched cell populations, we could not rule out that the signal may

464 originate from a small fraction of co-purified differentiated cells. We also performed *in situ*

465 hybridization against the neoblast marker *piwi-1* on cells dissociated from transfected animals

466 but failed to detect convincing cases of Nluc/*piwi-1* co-localization. Hence it is possible that

467 transfections of neoblasts are rare, or that upon transfection, neoblasts might lose *piwi-1*

468 expression, which is known to be sensitive to the cell cycle (Raz et al., 2021). These results

469 suggest that efforts need to be made either to identify transfection methods that are more

470 efficient at transfecting neoblasts specifically, or to better understand how transfection perturbs

471 neoblast identity. Finally, of the two most effective transfection reagents, one (Viromer mRNA)

472 is no longer commercially available. Since Trans-IT and Viromer are both cationic polymers,

473 other reagents with similar chemistries may provide substitutes for *in vitro* transfections. For *in*

474 *vivo* transfections, Trans-IT is most effective, remains commercially available, and thereby

475 represents the most promising route going forward towards planarian transgenesis.

16

Acknowledgements

Author Contributions

Conceptualization, R.N.H., U.W., A.F., J.C.R., and B.W.; Methodology, R.N.H., U.W., L.D., S.L.O., and H.L.; Investigation, R.N.H., U.W., L.D., and C.C.; Writing – Original Draft, R.N.H., J.C.R, and B.W.; Writing – Review & Editing, R.N.H., U.W., S.L.O., A.S.A., A.Z.F., J.C.R., and B.W., with input from all other authors; Supervision, N.A.M., A.Z.F., J.C.R, and B.W.; Funding acquisition: A.S.A., N.A.M., A.Z.F., J.C.R, and B.W.

Declarations of Interest

The authors declare no competing interests.

495   **Figures**

496

497
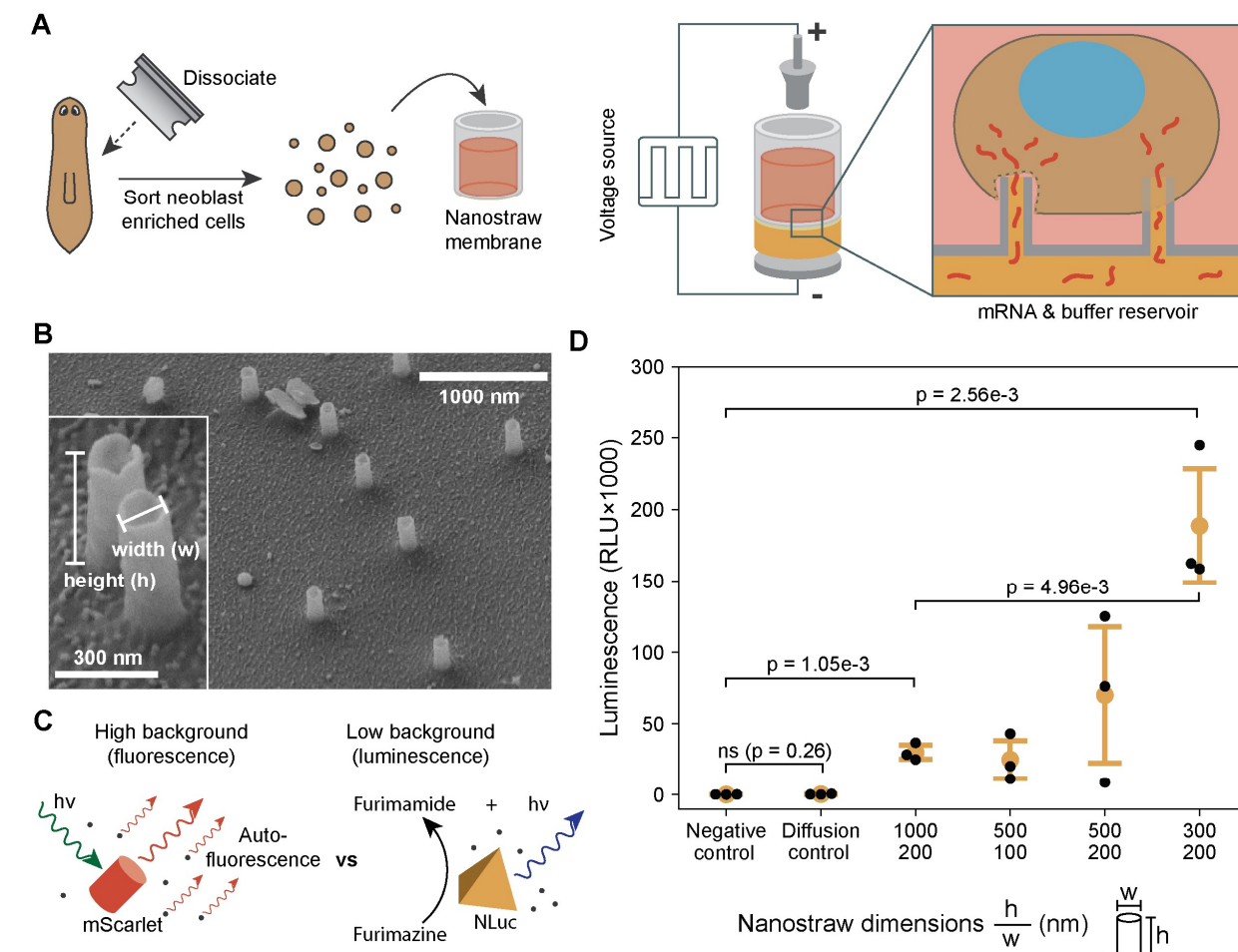
498   **Figure 1: Nluc mRNA delivered through nanostraws is expressed in planarian cells.**

499   (**A**) Schematics showing the steps of nanostraw delivery. In each experiment, 200,000 cells are

500   placed into a nanostraw cartridge and electroporated with square wave pulses between two

501   titanium electrodes.

502   (**B**) SEM images of nanostraws. Inset: a magnified view showing individual straws.

503   (**C**) Unlike autofluorescence, autoluminescence is absent in planarian tissues, making

504   luminescent reporters easy to detect.

505   (**D**) Luminescence from 200,000 cells at 24 hpt with sNluc1 mRNA. Cells are transfected using

506   three 45 s square wave pulse train of 35 V, 200 μs, and 40 Hz with 1 min between each cycle.

507   Negative control: nanostraw delivery with PBS alone. Diffusion: mock experiments without

508   applying electrical pulses. Luminescence is measured at room temperature with NanoGlo-Live

18

509   substrate by plate reader. Each data point represents one biological replicate which was

510   conducted on an independently isolated population of cells using nanostraws from the same

511   batch and mRNA synthesized in the same reaction. Error bars: standard deviation. Statistical

512   analysis is performed with one-way ANOVA ($p = 8.05\mathrm{e}{-5}$) in addition to two-sided Welch's t-

513   test to calculate p-values between pairs of conditions; ns: not significant ($p > 0.05$).
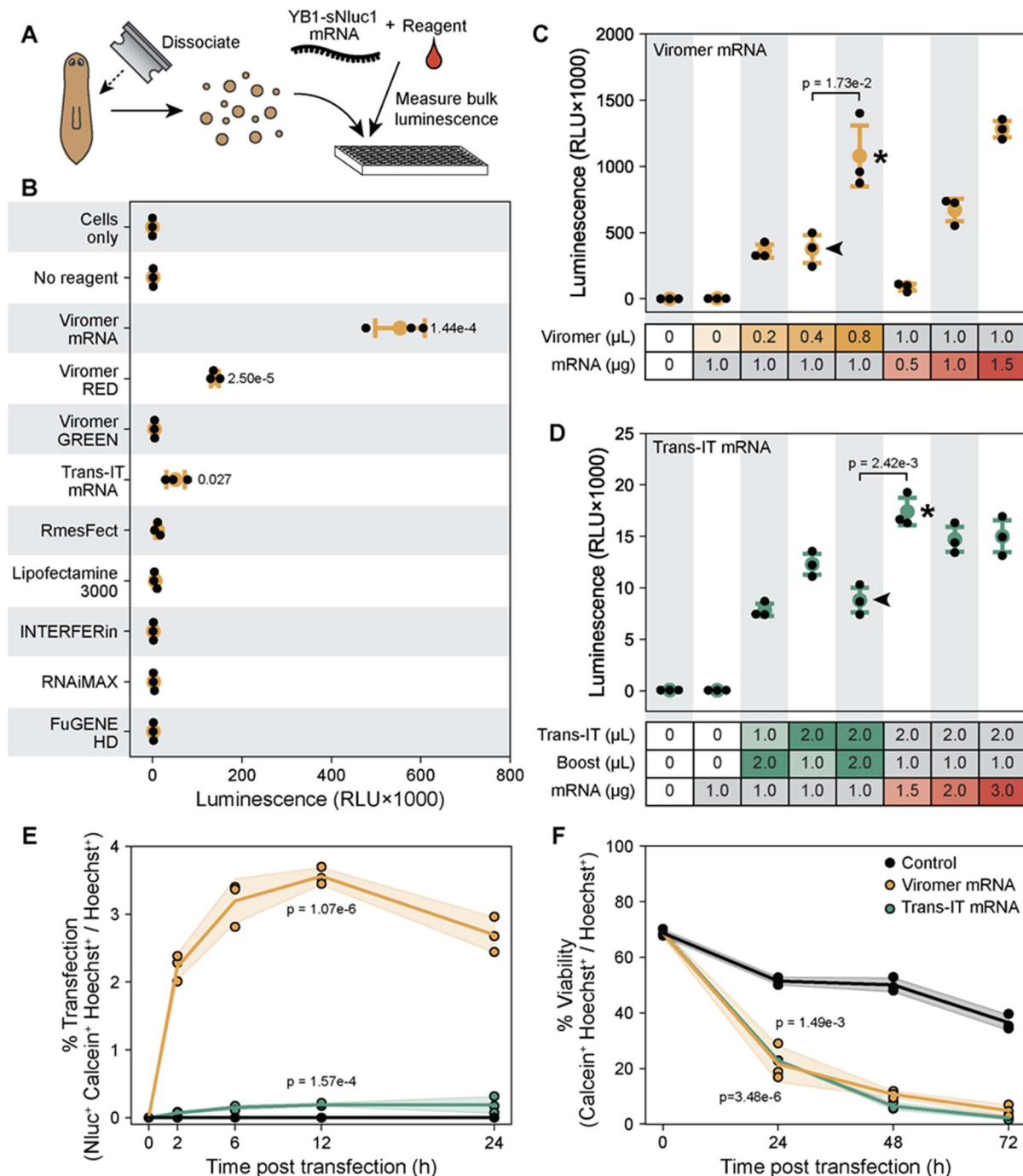
Figure 2: A screen identifies chemical reagents to efficiently transfect planarian cells.

(**A**) A diagram demonstrating the chemical transfection reagent screen pipeline.

(**B**) Luminescence from 200,000 cells transfected with 1 µg of YB1-sNluc1 mRNA delivered by

chemical transfection reagents, using the manufacturer's recommended protocols, assayed at 24

hpt (**Table S2**).

520   (**C-D**) Optimization of Viromer mRNA (**C**) and Trans-IT mRNA (**D**) transfections identifies

521   conditions with increased expression that are used for all following experiments (asterisk),

522   compared to the condition initially used in the screen (arrowheads). 200,000 cells are transfected

523   in each experiment and assayed at 24 hpt.

524   (**E**) Percentage of luminescent cells (Nluc$^+$Calcein$^+$Hoechst$^+$ / Hoechst$^+$) over the course of 24

525   hpt.

526   (**F**) Cellular viability (Calcein$^+$Hoechst$^+$ / Hoechst$^+$) over the course of 72 hpt. Cells in (**E**) and

527   (**F**) are transfected according to the optimal conditions found in (**C**) and (**D**) with either Viromer

528   (yellow), Trans-IT (green), or left untransfected (black). Cells are imaged on an Olympus LV200

529   luminescence microscope using a 20× air objective (Olympus, UPLXAPO20X). Cells are stained

530   with Hoechst 33342 (1 µM) and Calcein AM (1 µg/µL) and quantified using scanR Analysis

531   3.2.0. Luminescence is measured at room temperature with NanoGlo-Live substrate.

532   Statistics. Data points in (**B**) represent the mean of technical replicates (n = 3) for each biological

533   replicate. Data points in (**C-F**) represent technical replicates using mRNA prepared from the

534   same batch. Error bars: standard deviation. ANOVA: p = 2.08e-18 (**B**); p = 1.25e-9 (**C**); p =

535   2.05e-11 (**D**). p-values for pairwise comparison are calculated using two-sided Welch's t-test and

536   reported in the figure. In (**B, E, F**), comparisons are made by comparing experimental groups

537   with the negative control in which mRNA is delivered with no transfection reagent.
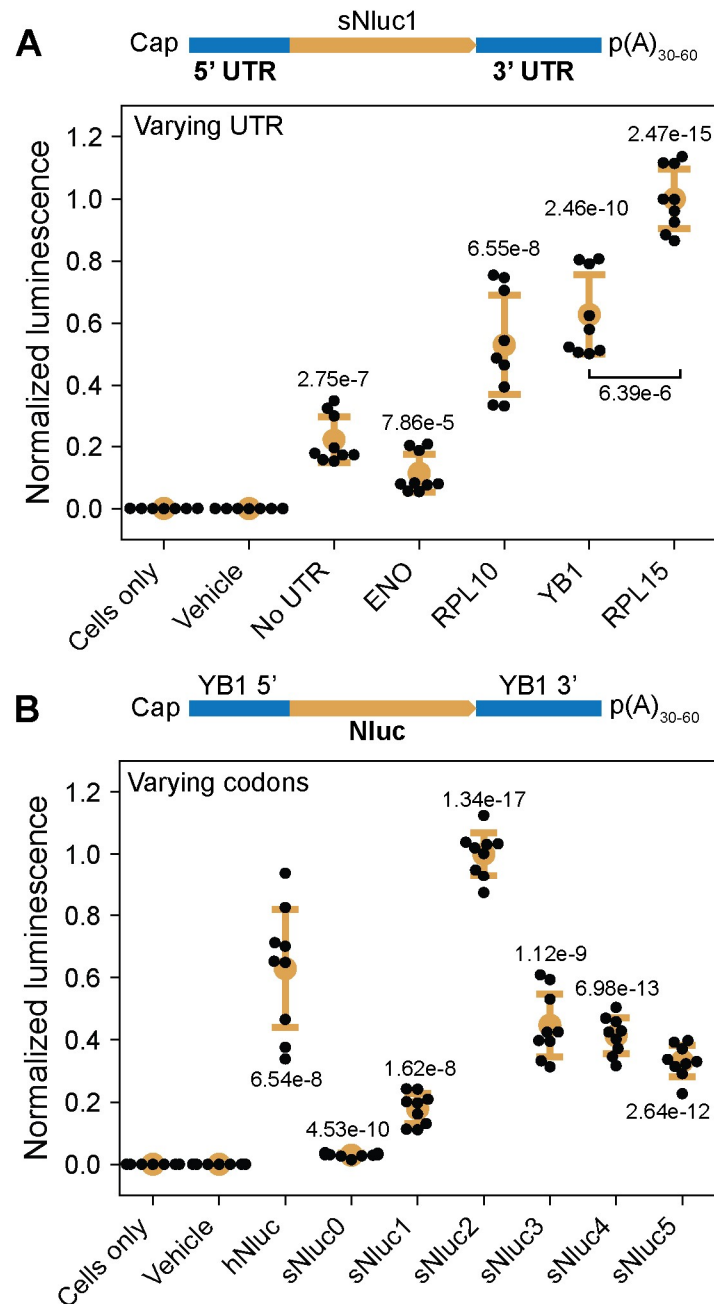
**Figure 3: Improving Nluc construct by altering UTR and codon bias.**

(**A**) Luminescence from transfections using constructs incorporating different endogenous 5' and 3' UTRs flanking sNluc1. No-UTR mRNA contains flanking attB1 and attP1 sequences used for cloning. UTRs were cloned from *ENO*, enolase (dd_Smed_v6_510_0_1); *RPL10*, ribosomal protein L10 (dd_Smed_v6_130_0_1); *YB1*, Y-box binding protein (dd_Smed_v6_52_0_1); *RPL15*, ribosomal protein L15 (dd_Smed_v6_193_0_1), which are identified using the gene annotation provided by PlanMine (Rozanski et al., 2019). We also choose to use UTRs from

546   shorter genes which mapped uniquely to the genome, allowing them to be more easily isolated

547   via PCR. All transfections in this figure are performed with 200,000 cells from whole dissociated

548   planarians using 0.8 µL Viromer and 1 µg mRNA per well and assayed 24 hpt at room

549   temperature using NanoGlo-Live substrate.

550   (**B**) Luminescence from alternative codon usage variants of Nluc flanked by YB1 UTRs. Codon

551   optimization schemes tested include utilizing only the most frequent codon for each amino acid

552   (sNluc0), the IDT online codon optimization tool (sNluc5) with manual adjustments to codon

553   usage (sNluc1), and random sampling of the codon table biased by the frequency of each codon

554   (sNluc2-4).

555   Statistics. All data points presented are technical replicates (n = 3) from independent biological

556   replicates (n = 3) each utilizing mRNA produced from independent *in vitro* synthesis reactions.

557   Luminescence measurements for each panel are normalized by the mean of the highest intensity

558   construct (panel **A**: RPL15; **B**: sNluc2). Error bars: standard deviation. ANOVA: p = 4.05e-31

559   (**A**); p = 2.98e-40 (**B**). p-values reported in the figure are calculated using two-sided Welch's t-

560   test between experimental groups and negative controls with cells only unless specified

561   otherwise in the figure.
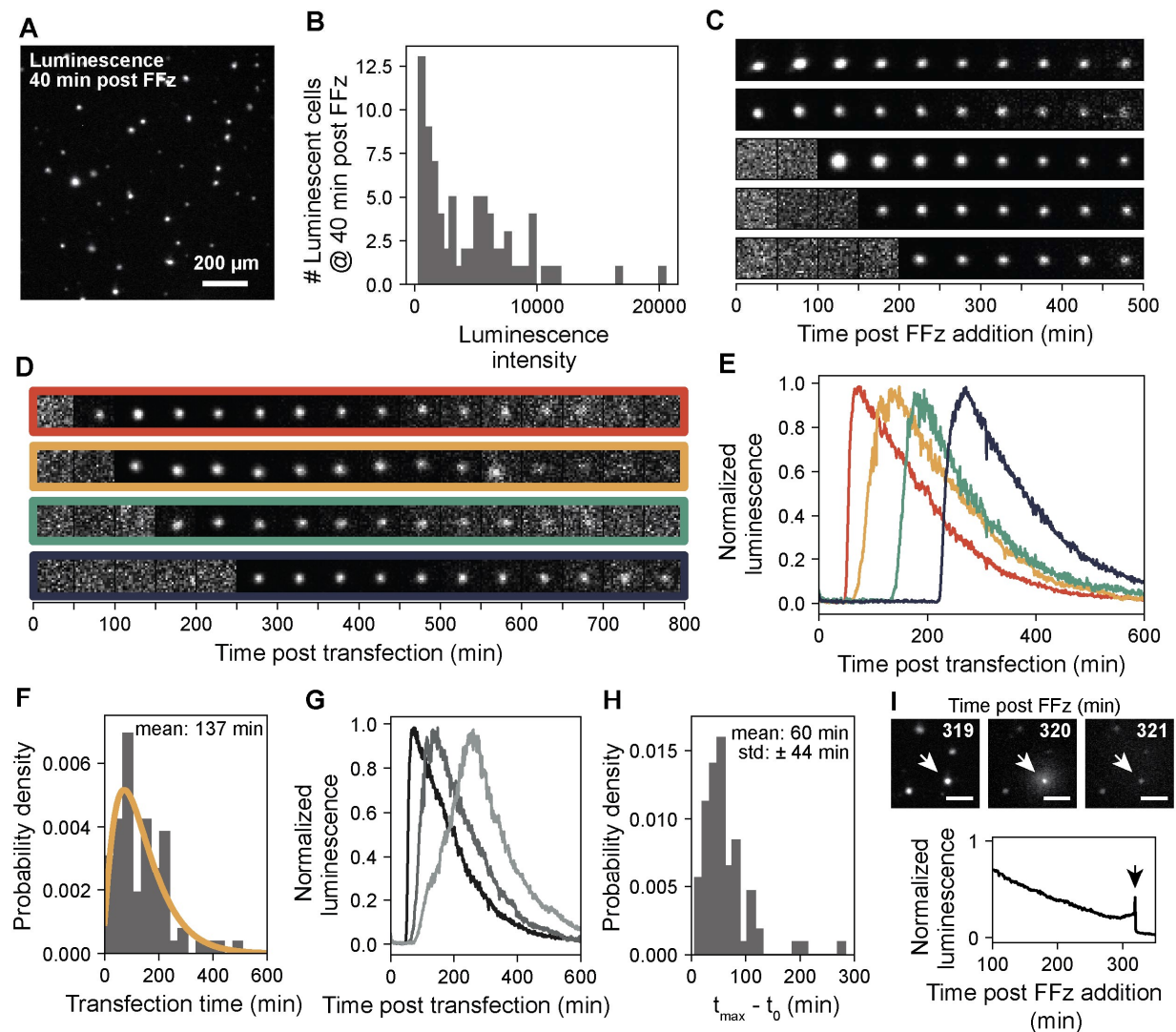
Figure 4: Time-lapse luminescence imaging reveals expression kinetics in single cells.

(**A**) Representative luminescence image of transfected bulk dissociated planarian cells. FFz (1:250) is added at 24 hpt and the image is acquired 40 min post FFz addition. All transfections reported in this figure use 0.8 µL of Viromer mRNA and 1 µg of RPL15-sNluc2 mRNA per 200,000 cells. All luminescence imaging is performed at room temperature with FFz substrate.

(**B**) The distribution of luminescence intensities of single cells treated as described in (**A**). Time of transfection is defined as the first time point when the total luminescence intensity of a cell exceeds ~3-fold above the background intensity.

(**C**) Examples showing temporal evolution of single-cell luminescence starting at 24 hpt when FFz is added. The three cells at the bottom are new transfections during imaging.

573   (**D**) Representative images showing luminescence intensity changes in individual cells. FFz

574   substrate and transfection complexes are added simultaneously at time 0, when imaging began

575   immediately.

576   (**E**) Time traces of single-cell luminescence intensities normalized against the maximum

577   intensity of each cell. Luminescence traces correspond to the cell bound by a frame of the same

578   color in (**D**).

579   (**F**) Distribution of transfection times. The curve is fit for a gamma distribution ($\alpha = 2.3$, $\beta =$

580   64.6).

581   (**G**) Example luminescence traces showing individual cells increasing in luminescence at

582   different rates.

583   (**H**) Distribution of the time intervals between the time of transfection (t_0) and the time of

584   maximum luminescence (t_{max}).

585   (**I**) (Upper) Images of a transfected cell undergoing cell death and releasing Nluc at 319 mpt

586   (immediately before rupture), 320 mpt (at the moment of rupture), and 321 mpt (after rupture).

587   Scale bars, 100 µm. (Lower) Normalized luminescence intensity of the cell shown above. The

588   arrow highlights the moment of rupture at 320 mpt.

589
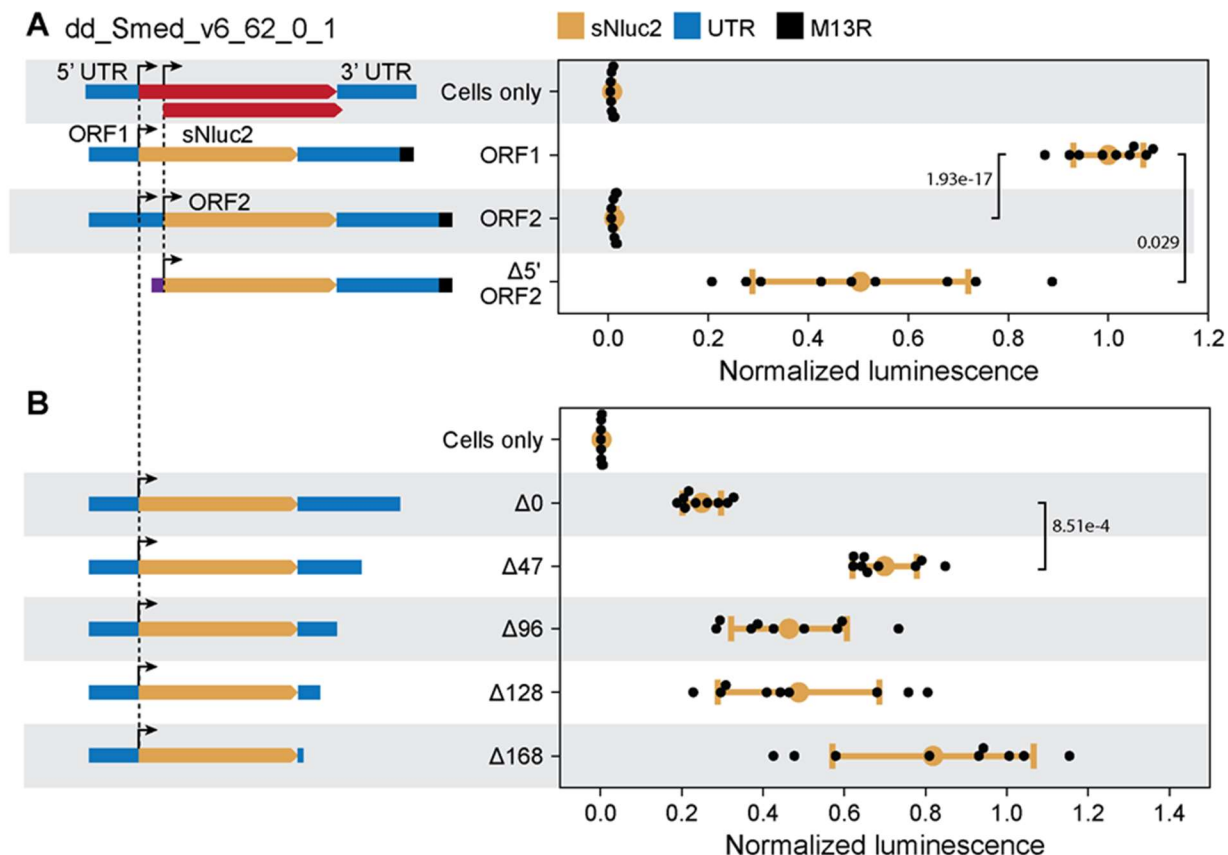
Figure 5: mRNA transfection enables studies of post-transcriptional regulation.

(**A**) Luminescence is detected with Nluc coding sequence beginning at ORF1 but not at ORF2 of dd_Smed_v6_62_0_1. Replacing the full-length 5' UTR of ORF2 with a synthetic UTR consisting of the attP1 sequence rescues the expression from ORF2. Note that there is a M13R synthetic sequence at the 3' end for all three constructs. In schematics, the dashed lines mark the beginning of ORFs. Luminescence is measured at room temperature with NanoGlo-Live substrate. All transfections in this figure are performed with 200,000 cells from whole dissociated planarians, using 0.8 µL Viromer and 1 µg mRNA per well, and assayed 24 at hpt. (**B**) Expression from the ORF1 construct with the 3' UTR successively truncated. Statistics. All data points presented are technical replicates (n = 3) from independent biological replicates (n = 3). All values reported are normalized to the expression of ORF1-sNluc2. Error bars: standard deviation. ANOVA: p = 1.83e-17 (**A**) p = 3.36e-7 (**B**). p-values for pairwise comparisons are calculated using two-sided Welch's t-test and reported in the figure.

26

603   **Figure 6**

604
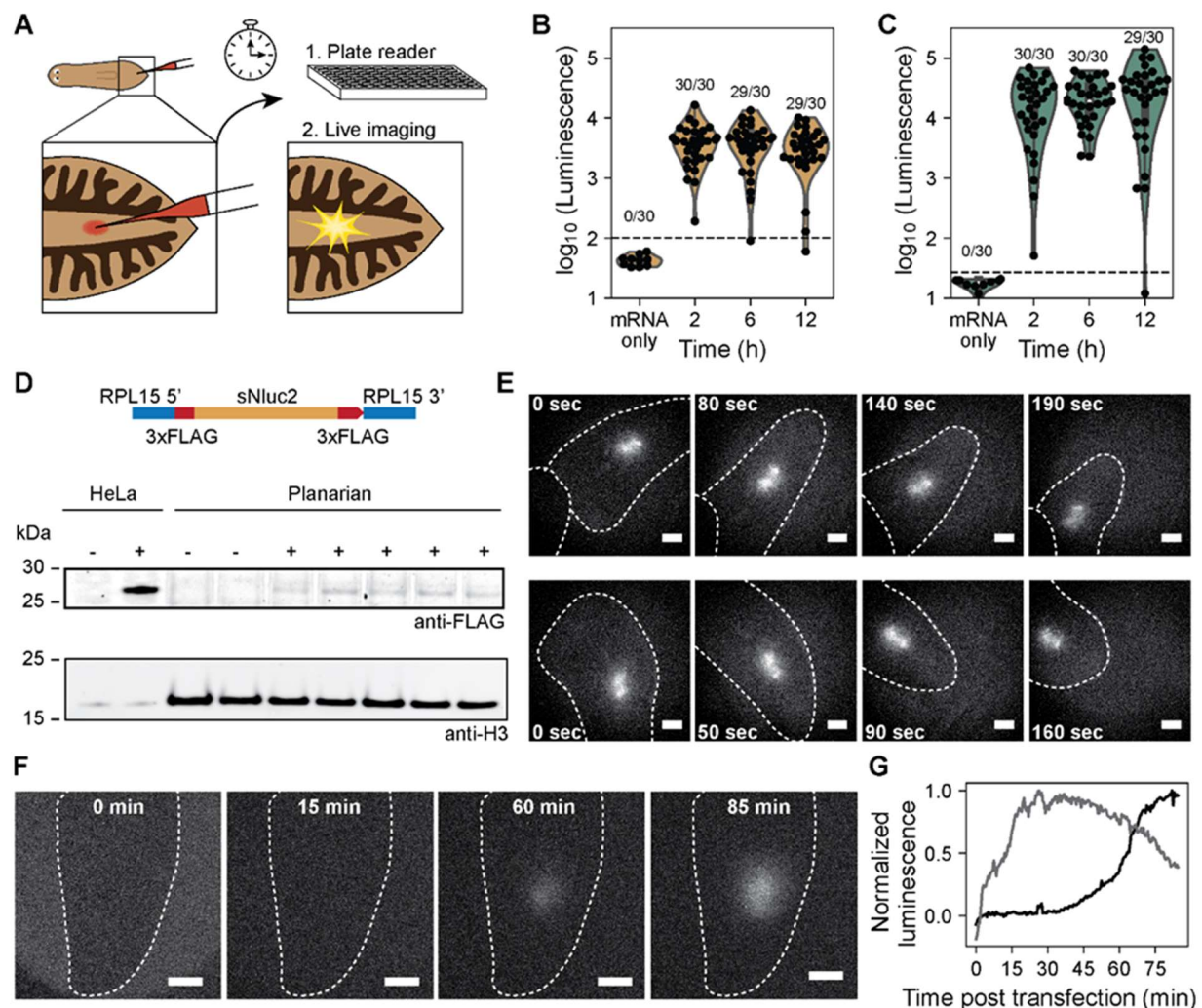
605   **Figure 6: Nluc expression in live animals**.

606   (**A**) Schematics showing the workflow of *in vivo* transfection experiments.

607   (**B-C**) Bulk luminescence is measured from dissociated tissues injected with mRNA complexed

608   with Viromer mRNA (**B**) or Trans-IT mRNA (**C**). Dashed lines: 3 standard deviations above the

609   background (based on the mRNA only condition) to discriminate negative and positive animals.

610   Numbers of positive animals out of all animals injected are reported for each time point.

611   Transfection complexes contain either 0.8 µL of Viromer, 1 µg of RPL15-sNluc2 mRNA, and

612   Viromer Buffer up to a final reaction volume of 25 µL, or 2 µL of Trans-IT, 1 µL of Boost, 1.5

613   µg of RPL15-sNluc2 mRNA, up to a final volume of 25 µL in L-15. For each transfection

614   reagent, 30 animals, from two independent experiments, are injected along the tail midline with

27

615   0.9 µL of transfection mix per time point. Transfected animals are dissociated, and luminescence

616   is measured at room temperature using NanoGlo lysis reagent.

617   (**D**) Western blot of Nluc protein from Trans-IT transfected planarian lysates. Animals are

618   injected along the tail midline and amputated at 12 hpt to collect the tails. Three tails are pooled

619   for each sample, from which protein is extracted. Hela cells are transfected with Trans-IT using

620   the same condition. Top: schematic diagram of the 6xFLAG-sNluc2 construct.

621   (**E**) Snapshots from a time-lapse video of two Trans-IT transfected animals imaged at 4 hpt.

622   Images are collected at 1 frame per min using 10 s exposure time and gain of 500 on an Andor

623   iXon DU-897 EMCCD with a 10× air objective (BoliOptics, N.A. = 0.25). Animals are

624   decapitated to reduce motility. Dashed lines: animal body boundary. Scale bars, 200 µm.

625   (**F**) Expression kinetics of *in vivo* transfection. Animals are transfected using Trans-IT and

626   allowed to rest for 30 min. Undiluted FFz substrate is injected into the gut and the animal is

627   embedded in anesthetic agarose solution (2% low melting point agarose, 0.1% chloretone,

628   1:5000 linalool) and imaged. Images show the luminescence intensity before (left) and during

629   (right) expression. Dashed lines: animal body boundary. Scale bars, 200 µm.

630   (**G**) Time traces of *in vivo* luminescence from two independently injected animals.

631   Luminescence is quantified as the difference between the total intensities from two equal-sized

632   regions centered at and above the injection site to subtract out ambient light intensity. The data is

633   normalized by the maximum luminescence.

Resource Availability

Lead Contact

Further information and requests for resources and reagents should be directed towards the lead contact, Bo Wang (wangbo@stanford.edu).

Materials Availability

Plasmids used in this study are available freely upon request and have been deposited to Addgene (#186753-#186774, and #187221). Though no longer commercially available, Viromer mRNA is available upon request while our limited supplies last. Nanostraw electro-delivery is presently being commercialized by NAVAN Technologies, who can be reached for inquiry. All species and strains of planarians used in this study are available upon request.

Data and Code Availability

- Original Western blotting images, raw plate reader values, and microscopy data have been deposited on Figshare.
- All data and code have been deposited on Figshare, and our GitHub accounts. DOIs are listed in the key resources table.
- Any additional information required to reanalyze the data reported in this paper is available from the lead contact upon request.

Experimental Models and Subject Details

Planarian Models

Asexual *S. mediterranea* strain CIW4 were reared in the dark at 20 °C and maintained in 0.5 g/L Instant Ocean (Carolina Biological Supply, Cat#671442) supplemented with 0.1 g/L sodium bicarbonate and were fed a diet of macerated calf liver once per week. *S. polychroa* strains were reared in the dark at 20 °C and maintained in 0.75× Montjuic Salts (1.2 mM NaCl, 0.75 mM CaCl$_2$, 0.75 mM MgSO$_4$, 0.075 mM MgCl$_2$, 0.075 mM KCl) supplemented with 0.1 g/L sodium bicarbonate and were fed a diet of macerated calf liver once per week.

29

Method Details

Planarian cell dissociation

Planarian cells were prepared by finely mincing 10-15 asexual *S. mediterranea* (5-7 mm in length) with a razor blade and suspending the tissue in CMF (Ca/Mg-Free media: 480 mg/L NaH_2PO_4, 960 mg/L NaCl, 1.44 g/L KCl, 960 mg/L $NaHCO_3$, 3.57 g/L HEPES, 0.24 g/L D-glucose, 1 g/L BSA, pH 7.4 in MilliQ H_2O). The tissue was rocked for 5 min, followed by gentle pipetting for 10 min for 3 times, or until the tissue was visibly homogenized. The cells were centrifuged at 250 g for 4 min, and the supernatant was removed and replaced with 1.5 mL of fresh CMF. The cell suspension was then serially filtered through 100, 70, 40, and 35-µm mesh strainers. The filtered cell suspension was centrifuged and transferred to Iso-L15 (1:1 Leibovitz's L-15 to MilliQ H_2O, 1× MEM nonessential amino acids, 1× antibiotic-antimycotic, 1× MEM vitamin solution, 1 mM Sodium Pyruvate, 2.5 g/L HEPES, 5% FBS, buffer to pH 7.8).

FACS

To isolate a neoblast-enriched X1FS population, an aliquot of sacrificial cells was stained with Hoechst 33342 (10 µg/mL, ThermoFisher, Cat#H3570) in CMF for 15 min, filtered, and sorted on a Sony SH800 with either the 100 or 130 µm sorting chip (Sony, Cat#LE-C3210, Cat#LE-C3213). Cells were gated for size using forward and side-scatter signals, then neoblasts were identified by gating, in linear scale, on cells with high Hoechst blue (Excitation: 405 nm, Emission 450/50 nm) and low Hoechst red (Excitation: 405 nm, Emission 600/60 nm) signal (Hayashi et al., 2006). Following the identification of the neoblast population using Hoechst fluorescence, unstained planarian cells were loaded and sorted into Iso-L15 medium using the X1FS gate overlaid on the forward and side-scatter. After sorting, the cells were centrifuged at 250 g for 5 min and resuspended in fresh Iso-L15.

Nanostraw electro-delivery

Nanostraws were acquired from NAVAN Technologies. Each nanostraw cartridge was loaded with 200,000 X1FS cells in 300 µL of Iso-L15 media and centrifuged at 300 g for 10 min to ensure close contact between straws and cells. For each cartridge, 3 µg of *in vitro* synthesized mRNA was diluted in PBS to a total volume of 35 µL and placed on the titanium anode, and a

693   cartridge was carefully lowered onto the mRNA solution. The titanium cathode was placed atop,

694   and the electro-delivery assembly was subjected to a 35 V, 200 μs, 40 Hz square wave pulse 3

695   times for 45 s each, with a 1 min rest in between pulses. Transfected cells were incubated at 20

696   °C in the dark for 24 hr before being transferred from the nanostraw cartridge to an opaque white

697   96 well plate (Greiner, Cat#655075) for assaying luminescence.

698

699   Chemical transfection

700   For *in vitro* experiments, dissociated planarian cells were suspended at a concentration of

701   0.88×10^6 cells/mL in Iso-L15 medium supplemented with 10 μg/mL ciprofloxacin (Sigma-

702   Aldrich, Cat#PHR1044). 225 μL of cell suspension was added to each well of white opaque (for

703   plate-reader assays) or glass bottom (for luminescence imaging) 96-well plates for a total of

704   approximately 200,000 cells per well. For the initial screen, each reagent was prepared as

705   specified in **Table S2**, and for all subsequent experiments, we utilized the optimal reagent ratios

706   identified in **Figures 2C-D**. After adding transfection complexes to each well, the cells were

707   incubated at 20 °C in the dark for 4-72 hr before assaying luminescence. Biological replicates

708   were performed by transfecting independently synthesized batches of mRNA, dissociated

709   planarian cells, and assembled transfection complexes. Within each biological replicate,

710   transfection mixes were split evenly across 3 parallel transfections of cells isolated from the

711   same dissociation.

712

713   For live animal injections, transfection mixes, prepared in the same manner as *in vitro* reactions,

714   were loaded into needles pulled from glass capillaries (WPI, Cat#1B00F-3) on a Sutter P90

715   needle puller with the following settings: pressure = 500, heat = 758, pull = 50, velocity = 70,

716   time = 200. Needles were loaded on a FemtoJet injection system (Eppendorf) or Sutter

717   XenoWorks injection system, and the needle tip was opened with forceps. Animals were placed

718   ventral-side up on moist filter paper placed on a cooled block. Animals were injected along the

719   tail midline with 900 nL transfection mix or until a bolus of injected fluid was visible and ceased

720   expanding. For ocular injections, animals were placed ventral-side down and injected

721   immediately posterior to the left eye cup. Animals were left to rest in the dark at 20 °C until

722   assaying 4-24 hpt.

723

Luciferase plate assay

For dissociated cells, luminescence was measured using the NanoGlo-Live Cell Assay (Promega, Cat# N2011). NanoGlo-Live substrate was added to NanoGlo buffer at a ratio of 1:20, and 25 µL of reagent was added to 250 µL of transfected cells. NanoGlo-Live reagent was also added to negative control conditions before assaying to ensure a consistent luminescence baseline.

For live planarians, each injected animal was individually dissociated by finely mincing with a razor blade and suspending the tissue in 250 µL Iso-L15 medium just prior to assaying. The resuspended tissue was transferred to an opaque white 96-well plate. Nluc expression was measured using the NanoGlo Luciferase Assay System (Promega, Cat# N1110). Substrate was added to the NanoGlo lysis buffer at a ratio of 1:50 and 100 µL of reagent was added to the cells. Cells were lysed by pipetting up and down 10 times or until the tissue was visibly homogenized.

Gaussia luciferase (Gluc) was assayed using the Pierce™ Gaussia Luciferase Glow Assay Kit (ThermoFisher, Cat#16160) according to the manufacturer's instructions. To measure luminescence from supernatant and cellular pellets, 250 µL of supernatant was carefully transferred to a fresh 96-well plate, then the remaining cells were resuspended in 250 uL of CMF. The resuspended cells were then transferred to a fresh 1.5 mL Eppendorf tube and were centrifuged at 250 g for 4 min. The supernatant was discarded, and the cells were then resuspended in 250 µL of Iso-L15 and transferred to an opaque white 96-well plate.

Luminescence was measured on a plate reader (BioTek Synergy™ HTX for collecting data presented in Figures 1, 3, 5, S5, S8, S12, S14; BioTek Synergy™ Neo2 for Figures 2C-D, 6B-C, S3, S13; and EnVision Microplate Reader for Figure 2B). Integration time was set at 1 s and the digital gain was kept consistent on each instrument for all experiments. All assays were performed at room temperature and luminescence was measured quickly after substrate was added to all wells.

Luminescence imaging setup

Luminescence imaging was performed on an LV200 Bioluminescence Imaging System (Olympus) equipped with a 20× air objective (Olympus: UPLXAPO20X, N.A. = 0.8), a 60× oil

32

755   immersion objective (Olympus: UPLXCAPO60XO, N.A. = 1.42), and a liquid-cooled

756   Hamamatsu C9100-24B EMCCD camera (1024×1024 pixels). All images taken with the LV200

757   were acquired with an exposure of 60 s and a gain of 300 unless otherwise specified.

758

759   Images were also acquired with a custom-built luminescence microscope, modified from Kim et

760   al., 2017, which utilizes an Andor iXon DU-897 EMCCD camera (512×512 pixels), a

761   HIKROBOT MVL-HF5024M-10MP 50mm tube lens, and either a 10× air (BoliOptics:

762   BM13013331, N.A. = 0.25), a 20× air (BoliOptics: BM03023431, N.A. = 0.4), or a 100× oil

763   (Carl Zeiss: 1084-514, N.A. = 1.45) objective. All images taken with the custom luminescence

764   microscope were acquired with an exposure time of 30 s and gain of 500 unless otherwise

765   specified. Micromanager 1.4 was used to operate the microscope.

766

767   Luminescence imaging *in vitro*

768   Nluc expression was detected using the NanoGlo-Live Cell Assay. A 35 mm glass-bottom dish

769   (WPI, Cat#FD3510-100) or a glass bottom 96-well plate (Cellvis, Cat#P96-1-N) were coated

770   with 0.5 mg/mL Concanavalin A (Sigma-Aldrich, Cat# L7647) for 2 hr, washed, and air dried.

771   Transfected cells were transferred to coated dishes in a total of 250 µL of Iso-L15 and allowed to

772   adhere to the glass surface for 1 hr. NanoGlo-Live substrate was added to NanoGlo buffer at a

773   ratio of 1:20, and 25 µL of reagent was added to 250 µL of transfected cells. Cells were imaged

774   at room temperature with either an LV200 Bioluminescence Imaging System (Olympus) with a

775   60× oil immersion objective (Olympus), or the custom-built luminescence microscope equipped

776   with a 100× oil immersion objective (Carl Zeiss).

777

778   Quantification of transfection efficiency and viability were measured by staining transfected

779   cells with Calcein AM (1 µM final concentration), propidium iodide (PI) (1 µg/µL final

780   concentration), and Hoechst 33342 (1 µg/µL final concentration). The cells were imaged on an

781   LV200 with a 20× air objective (Olympus), and individual cells were classified using scanR

782   Analysis 3.2.0 (Olympus). Transfected cells were classified as being positive for Calcein,

783   Hoechst, and Nluc. Viability was quantified by classifying live cells as positive for both Calcein

784   and Hoechst. Total cells were quantified by Hoechst positive nuclei.

785

Luminescence imaging *in vivo*

For *in vivo* imaging, animals were incubated in 100 µL of 1× Instant Ocean supplemented with 1% DMSO and 1:20 NanoGlo-Live substrate for 15 min at room temperature. The animals were then placed on glass bottom dishes cooled on ice. Excess water was wicked away, and the animals were embedded in 1.5-2% low-melt agarose gel (ThermoFisher, Cat#16520050) supplemented with 1:5000 linalool (Sigma-Aldrich, Cat#L2602) and 1:20 NanoGlo-Live substrate. A coverslip was placed over the agarose to prevent lensing. The animals were imaged using an LV200 with a 20× air objective (Olympus) at an exposure of 60 s and gain of 300.

Time-lapse imaging *in vitro*

Bulk dissociated planarian cells were transfected with 0.8 µL of Viromer and 1 µg RPL15-sNluc2 mRNA. Cells were either imaged immediately or allowed to incubate for 24 hr at 20 °C. Substrate was prepared by diluting NanoGlo In-Vivo substrate (FFz) (Promega, Cat#CS320501) 1:50 in Iso-L15, then 25 µL of this solution was added to the 250 µL of transfected cell media. Cells were imaged at room temperature on a custom-built luminescence microscope with a 20× air objective (BoliOptics, N.A. = 0.4) at 1 frame per min with an exposure of 30 s and gain of 500. Individual cells were automatically segmented using Python 3.8 and scikit-image (see Code and Data Availability).

Time-lapse imaging *in vivo*

To image unrestrained animals, they were allowed to incubate at 20 °C for 4 hr post injection, then amputated immediately anterior to the injection site. The animals were placed in a solution of 1× Instant Ocean containing 1:20 NanoGlo In-Vivo substrate (FFz) and imaged at a rate of 6 frames per min with an exposure of 10 s and gain of 500.

For measuring expression kinetics *in vivo*, animals were allowed to rest for 15 min post injection and re-mounted ventral-side up on moist filter paper over a cool block. Undiluted FFz was injected into the gut until at least one posterior gut branch had visibly filled with yellow substrate, then the animal was placed ventral-side down on a cooled glass-bottom dish. Excess water was wicked away before immobilization. Anesthetic agarose was prepared by mixing 2% agarose in 1% chloretone (Sigma-Aldrich Cat# 112054) dissolved in 1× Instant Ocean

817   supplemented with 1:5000 linalool. The agarose solution was cooled to 37 °C and allowed to

818   cool further just before gelling began, and drops were added on and around the animal to

819   immobilize it. Animals were imaged at room temperature on a custom-built luminescence

820   microscope with a 10× air objective (BoliOptics, N.A. = 0.25) at 2 frames per min with an

821   exposure of 30 s and gain of 500.

822

823   Cloning

824   To generate a plasmid for *in vitro* transcription and harvesting the UTR sequences, we first

825   amplified the backbone of pDONOR221 (ThermoFisher, Cat#12536017) using primers BW-NH-

826   104-105 (all primer sequences are provided in **Table S4**), as well as the LacZ cassette from

827   pUC19 (Addgene #50005) with a T7 promoter sequence followed by a BsaI restriction site for

828   subsequent cloning steps, all flanked between BbsI restriction sites and M13 forward and M13

829   reverse primer sites (for *in vitro* transcription template production) using primers BW-NH-106-

830   107. The amplified backbone was digested with BsaI-HFv2 (NEB, Cat#R3733S) and the LacZ

831   insert was digested with BbsI-HF (NEB, Cat#R3539S). The digested backbones were purified

832   using the Zymo Clean and Concentrate kit (Zymo, Cat#D4004). The purified fragments were

833   ligated together using T4 DNA Ligase (NEB, Cat#M0202S) to create pNHT7 (**Figure S6A**).

834

835   We cloned the gene of interest (GOI) from a pool of planarian cDNA using primers (BW-NH-

836   108-125) containing BsaI restriction sites to produce overhangs compatible with pNHT7. The

837   amplicons were purified using the Zymo Clean and Concentrate kit and then inserted into

838   pNHT7 via a golden gate reaction containing 40 ng of backbone and 20 ng for each insert to be

839   cloned in a 20 µL reaction volume containing 2 µL T4 Ligase Buffer, 1 µL T4 DNA Ligase, and

840   1 µL BsaI-HFv2 to produce pNHT7::GOI (**Figure S6B**).

841

842   Finally, to insert a reporter between the 5' and 3' UTRs, we amplified pNHT7::GOI with

843   outward facing primers (BW-NH-128-139) which bind to the end and beginning of the 5' and 3'

844   UTRs respectively containing the BsaI restriction sites. The reporter was then amplified to

845   append compatible BsaI restriction sites using primers BW-NH-174-185 and inserted between

846   the two UTR sequences via a golden gate reaction. The resulting plasmids were amplified with

847   M13 forward and M13 reverse primers to produce linear template for *in vitro* transcription

848   reactions (**Figure S6C**).

849

850   *In vitro* transcription

851   Linearized templates for *in vitro* transcription were amplified using Phusion Polymerase

852   (ThermoFisher, Cat#F531L) in two parallel 50 µL format reactions containing 10 µM M13F/R

853   primers (**Table S4**) and 25 ng of template DNA. The two reactions were pooled and purified

854   using the Zymo Clean and Concentrator kit, and the templates were eluted in 8 µL of RNase-free

855   water. For the 'UTR hacking' experiments (**Figure 5**), PCRs were performed as described but

856   replacing the M13R primer for an oligo which primes directly to the 3' UTR (**Table S4**).

857   Expected concentrations should range from 200-300 ng/µL.

858

859   *In vitro* transcription (IVT) was performed using the T7 mScript™ Standard mRNA Production

860   System (CELLSCRIPT, Cat#C-MSC100625) according to the manufacturer's protocol, opting

861   for a 1.5 hr incubation during T7 transcription, a 2 hr incubation for 5' capping, and a 1 hr

862   incubation for poly-A tailing, all performed at 37 °C. RNA purification was performed by adding

863   600 µL of ethanol and 50 µL of 10 M ammonium acetate to 200 µL of IVT reaction, and

864   allowing to precipitate overnight at -20 °C. The precipitated mRNA is then centrifuged at 21,000

865   g for 30 min at 4 °C. The pellet was then rinsed twice with 70% ethanol and allowed to air dry

866   before being resuspended in 60 µL of nuclease-free water. A standard 60 µL reaction typically

867   yields 60 µg of mRNA. For expected results, see **Figure S7**. For mRNA containing m1Ψ, the

868   rNTP mix provided in the CELLSCRIPT kit was substituted for a mixture of rNTPs containing

869   10 mM rGTP, 10 mM rCTP, 10 mM rATP, and 10 mM m1Ψ (TriLink, Cat#N-1019-1). The IVT

870   reaction can be scaled down by a half, though precipitation was done with the full volumes

871   described here.

872

873   Preparation of protein lysates

874   At 12 hpt, animals were washed twice with 1× Instant Ocean and decapitated to enrich for the

875   injected regions. Three tails were pooled for each sample, transferred to a 1.5 mL tube and 80 µL

876   Urea lysis buffer (9 M Urea, 100 mM NaH_2PO_4, 10 mM Tris-Base, 2 % w/v SDS, 130 mM DTT,

877   1mM $MgCl_2$) was added. Animals were immediately lysed with a motorized pestle, followed by

878 incubation at room temperature for 20 min to fully denature proteins. Cellular debris was then

879 pelleted by centrifugation at 21,000 g for 15 min and supernatant was moved to a fresh 1.5 mL

880 tube. Small aliquots from the protein lysates were diluted 1:10 in MilliQ H_2O to quantify protein

881 concentration based on 280 nm absorbance using a spectrophotometer. 20 µL of 5× LDS buffer

882 (530 mM Tris HCl, 700 mM Tris-Base, 10 % w/v LDS, 50 % w/v glycerol, 2.55 mM EDTA, 500

883 mM DTT, 0.11 mM SERVA Blue G250, 0.875 mM Phenol Red, pH 8.5) was then added to each

884 sample.

885

886 SDS-PAGE and Immunoblotting

887 SDS-PAGE and Western blotting were performed using a XCell SureLock Mini-Cell and XCell

888 II system (Invitrogen, Cat#EI0002). 40 µg total protein from planarian lysate or 5 µg total

889 protein from HeLa cell lysate were loaded per well onto a NuPAGE 4-20 % BisTris gel

890 (ThermoFisher, Cat#NP0321BOX) and run in 1× MOPS buffer (ThermoFisher, Cat#NP0001) at

891 125 V for 110 min. Proteins were blotted onto a 0.45 µm nitrocellulose membrane (Merck,

892 Amersham Protran, Cat#GE10600002) for 2 hr at 4 °C and 30 V. Membranes were washed with

893 PBSTw (PBS supplemented with 0.1 % Tween 20) twice followed by blocking for 1 hr in PBS

894 with 5 % (w/v) soy protein isolate (Powerstar Food, Cat#psf-1131). Membranes were then

895 incubated overnight at 4 °C on a horizontal shaker with primary antibody in PBSTw

896 supplemented with 0.5 % (w/v) soy protein isolate. Membranes were then washed 4 times with

897 PBSTw over 1 hr and incubated with secondary antibody in PBSTw with 5 % (w/v) soy protein

898 isolate for 2 hr on a horizontal shaker. Membranes were again washed 4 times with PBSTw over

899 1 hr, rinsed with PBS twice and dried for 1 hr. Images were acquired on an Amersham Typhoon

900 imaging system (Cytiva).

901

902 Mouse anti-FLAG-M2 (Merck, Cat#F3165; dilution 1:5000) and Rabbit anti-Histone3 (abcam

903 Cat#ab1791; dilution 1:30000) were used as primary antibodies. Goat anti-mouse-CF770

904 (Biotium, Cat#20077; dilution 1:10000) and goat anti-rabbit-CF680 (Biotium, Cat#20067;

905 dilution 1:10000) were used as secondary antibodies.

906

Quantification and Statistical Analysis

All statistical tests were performed using Python 3.8 and the SciPy 1.8.0 stats package in Jupyter notebooks which have been deposited to Figshare (see Data and Code Availability). Images were processed in ImageJ 1.53k, and single-cell segmentation and quantification was performed in scanR Analysis 3.2.0 (Olympus).
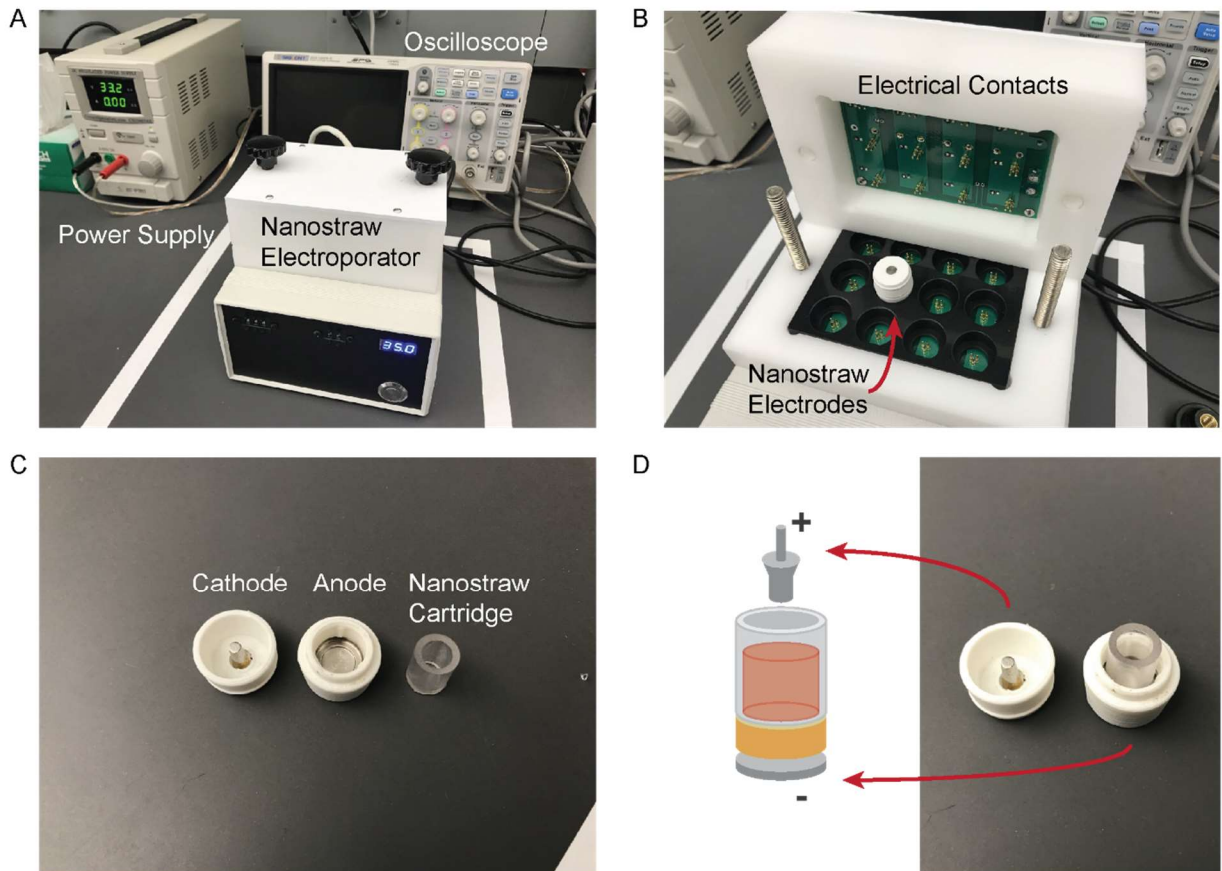
912   **Supplemental Information**

913

914   **Figure S1-S14**

915   **Table S1-S4**

916   **Video S1-S4**

917   **File S1**

918 **Supplemental Figures**

919

920

921 **Figure S1: Nanostraw electro-delivery device, Related to Figure 1.**

922 (**A**) A photograph of the nanostraw device. In frame is the power supply (left), the oscilloscope,

923 which is used to monitor the square wave pulses (top right), and the nanostraw electroporator

924 device (center bottom) showing the dials to set the pulse width, duration, and voltage.

925 (**B**) An interior view of the nanostraw device, showing the electrical contacts which interface

926 with the nanostraw electro-delivery cartridge and carry the electrical pulses to the titanium

927 electrodes on the top and bottom of the cartridge.

928 (**C**) Individual components of the nanostraw cartridge, showing the cathode, which dips into the

929 cell culture medium from above, the anode, which sits just below the buffer and mRNA to be

930 delivered, and the nanostraw membrane, which is inserted atop the buffer and anode.

931 (**D**) A demonstration of a nanostraw membrane placed within the cartridge.

40
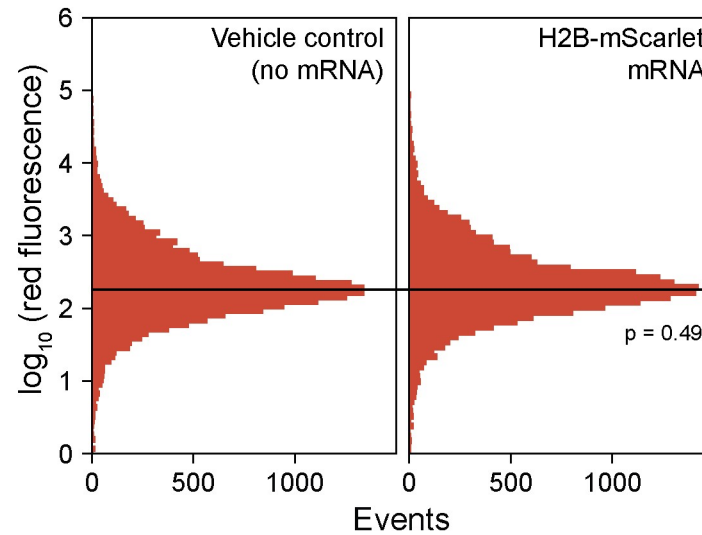
Figure S2: **Autofluorescence in planarian cells, related to Figure 1.**

Histogram of red fluorescence (Excitation: 405 nm, Emission: 600/50 nm) of cells after

nanostraw delivery measured by flow cytometry. Both samples show nearly identical

distributions. Statistical insignificance (p = 0.49, two-sided Welch's t-test) is established by

bootstrapping, which calculates the p-value for 10,000 random subsamples of 100 cells between

both distributions.
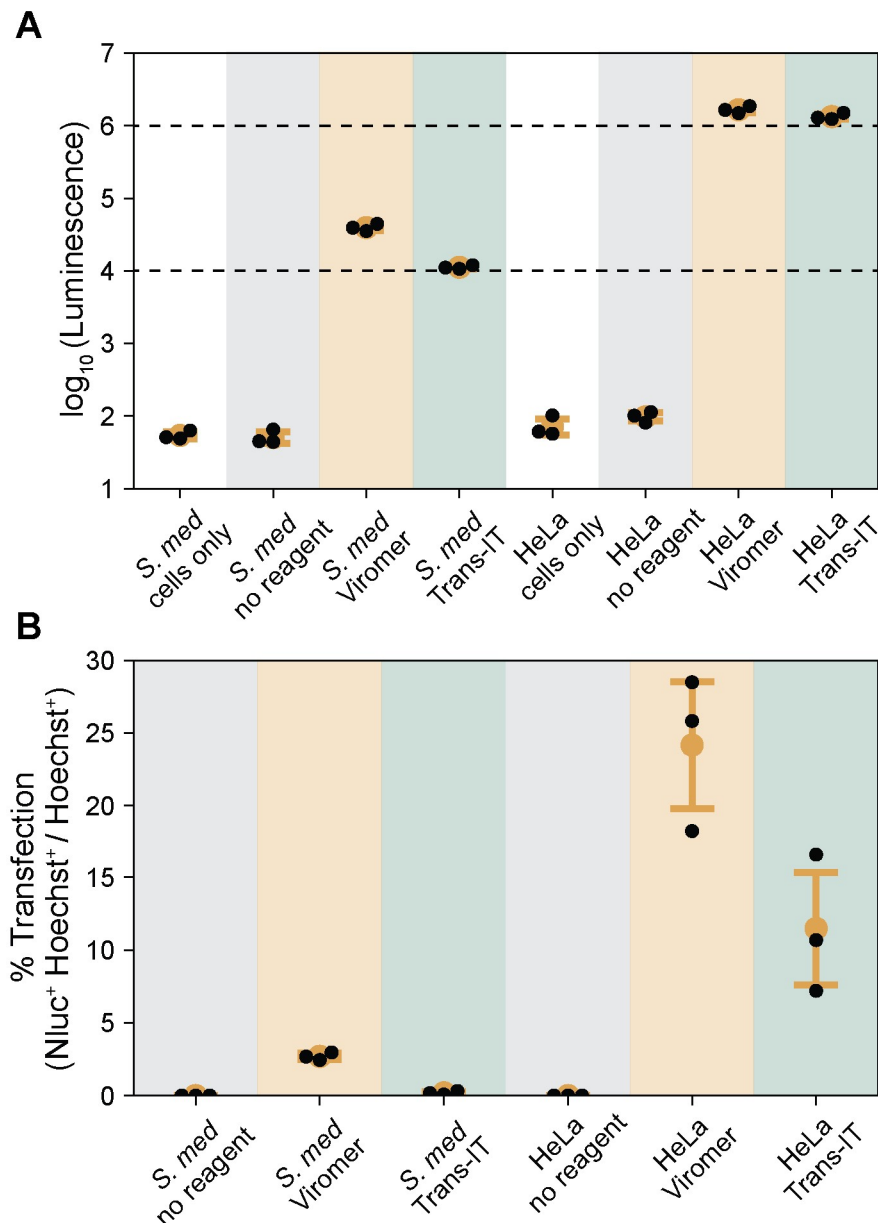
Figure S3: Comparisons of Nluc expression in planarian and HeLa cells, related to Figure 2.

(**A**) Bulk luminescence of RPL15-sNluc2 transfected planarian and HeLa cells. All transfection are performed with 200,000 cells using optimal conditions identified in **Figure 2C-D** for planarian cells and **Table S2** for HeLa cells, and assayed 24 hpt at room temperature using NanoGlo-Live substrate. Dashed lines highlight 10^4 and 10^6 RLU.

(**B**) Percent transfection efficiencies (Nluc$^+$Hoechst$^+$/Hoechst$^+$) of transfected planarian and HeLa cells.
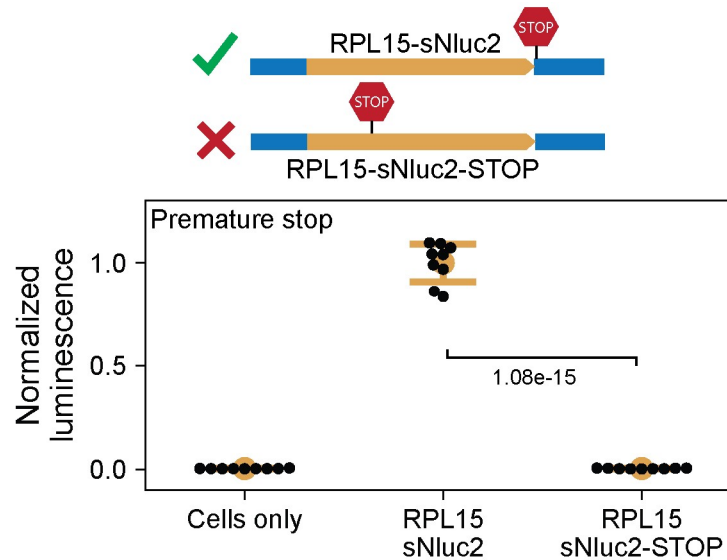
42

948   Statistics. All data points presented are technical replicates using the same batch of mRNA. Error

949   bars: standard deviation. ANOVA p = 1.35e-14 (**A**); p = 1.21e-6 (**B**).
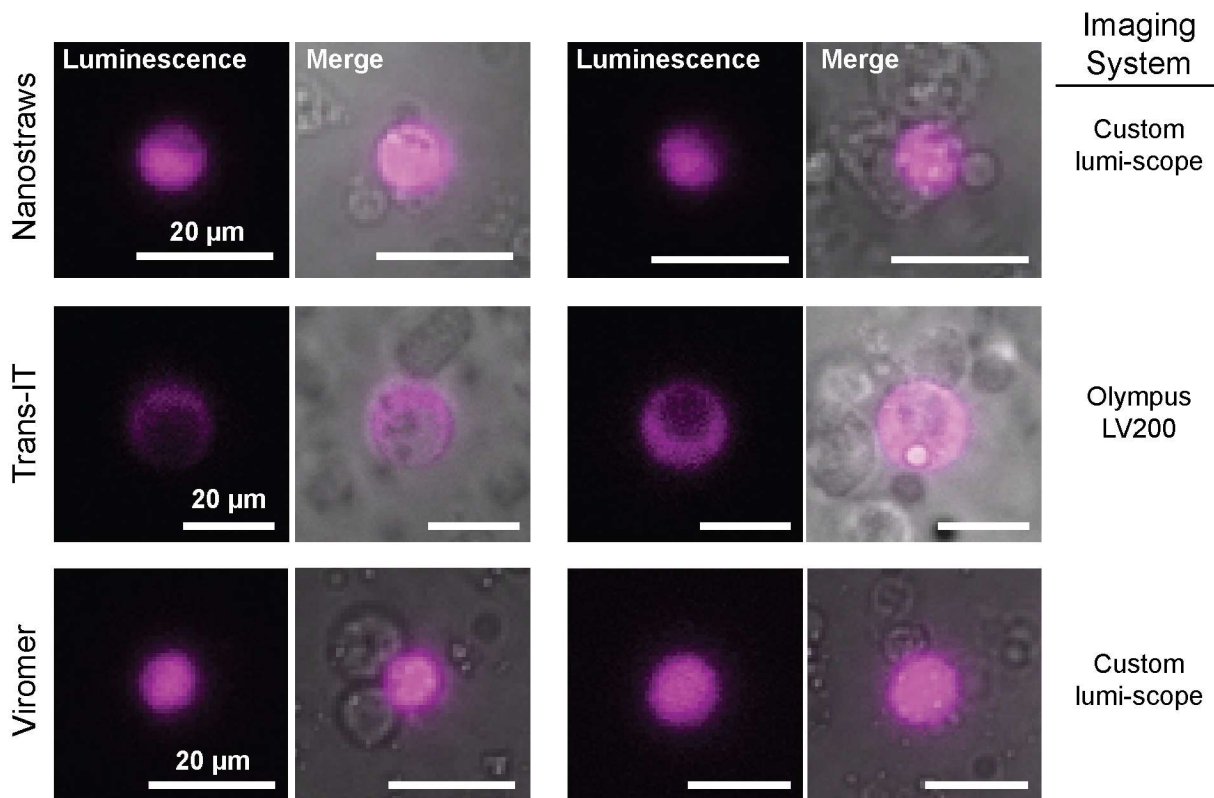
Figure S4: Luminescence imaging of transfected cells, related to Figure 2.

Representative images of planarian cells transfected with either nanostraws (300 nm × 200 nm, 35V, 200 μs, 40 Hz) delivering RPL15-sNluc2 mRNA, Trans-IT delivering YB1-sNluc1 mRNA, or Viromer delivering RPL15-sNluc2, utilizing optimized transfection conditions for each method. Cells are imaged at 20 °C on either an Olympus LV200 luminescence microscope with a 100× oil immersion objective (Olympus: UPLXAPO100XO) or the custom-build luminescence microscope with a 100× oil immersion objective (Carl Zeiss: 1084-514) to observe cellular localization of luminescence (magenta).

959

Figure S5: Premature stop codon abolishes Nluc expression, related to Figure 2.

Luminescence from 200,000 dissociated planarian cells transfected with Viromer and RPL15-sNluc2 mRNA containing either a stop codon at the end of the 516 amino acid sequence or a variant containing a premature stop codon at residue 16. Luminescence is assayed 24 hpt. Statistics. All data points presented are technical replicates (n = 3) from independent biological replicates (n = 3) using mRNA produced from independent *in vitro* synthesis reactions. Luminescence measurements are normalized to the mean luminescence of RPL15-sNluc2. Error bars: standard deviation. ANOVA: p = 1.22e-18. p-value reported in the figure is calculated from a two-sided Welch's t-test.

969
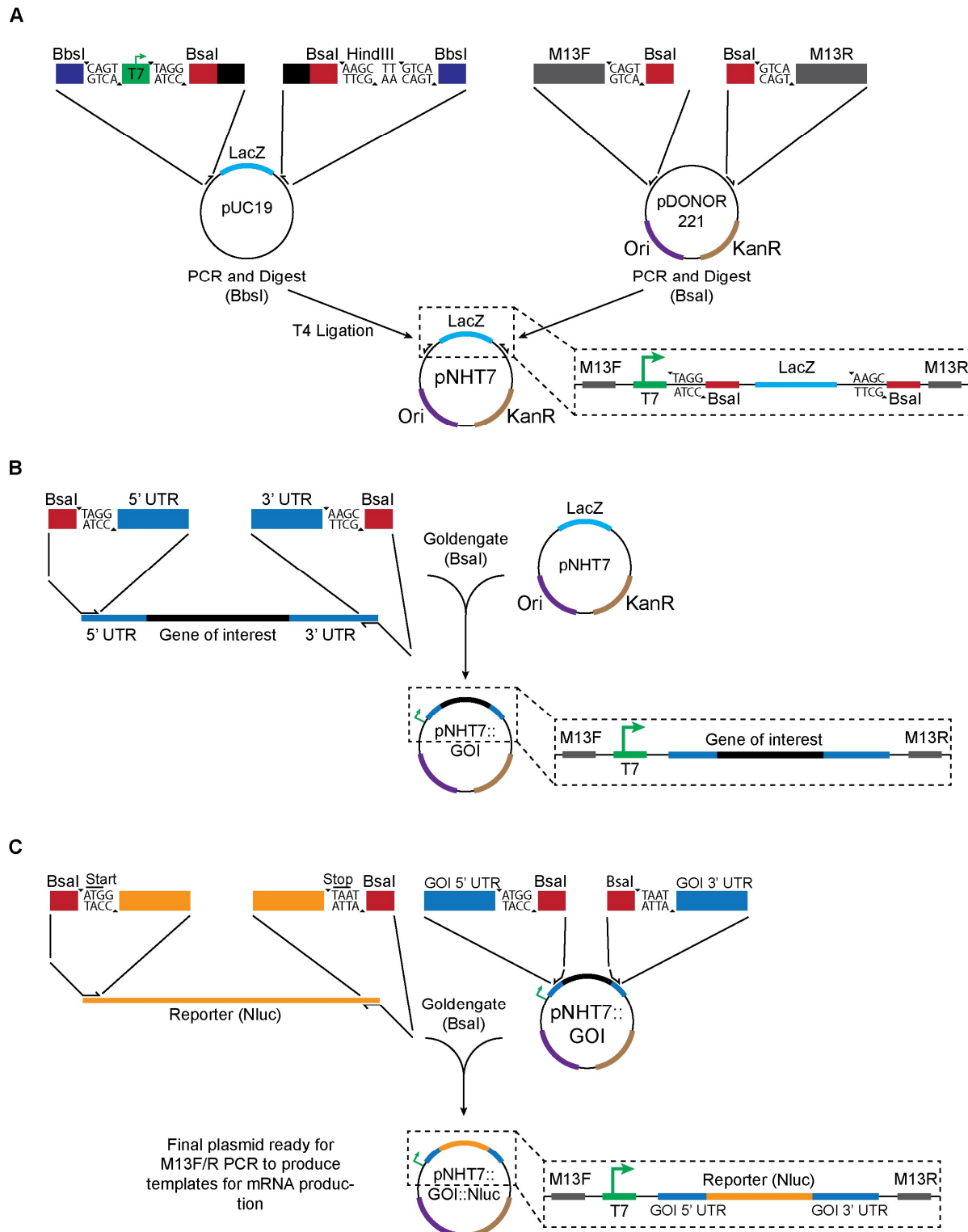
Figure S6: Cloning methodology, related to Figure 3.

971   (**A**) A diagram showing the steps of generating pNHT7, the base vector used to clone

972   endogenous planarian genes. The overall design is a LacZ cassette, derived from pUC19, flanked

973   by BsaI restriction sites, which allow for subcloning of planarian genes into pNHT7. Upstream is

974   a T7 promoter, which allows for IVT, and all of these are flanked by M13 forward and reverse

975   primers, which are used to generate linearized templates for IVT through PCR. The backbone for

976   pNHT7 is derived from the backbone from pDONOR221.

977   (**B**) Isolating the 5' and 3' UTRs of a GOI from cDNA uses primers containing pNHT7

978   compatible BsaI restriction sites followed by 5' and 3' UTR sequences of the GOI. After

979   amplification, the fragment containing the GOI can be cloned into pNHT7 though a standard

980   golden gate reaction.

981   (**C**) The Nluc reporter is inserted between the UTR sequences by using primers containing BsaI

982   restriction sites to prime the 5' and 3' ends of the reporter as well as outward facing primers

983   which add complementary BsaI restriction sites and prime the end of the 5' UTR and beginning

984   of the 3' UTR for the gene captured in pNHT7. These two amplicons can then be purified and

985   assembled via a golden gate reaction. All primer sequences are provided in **Table S4**.

47

986
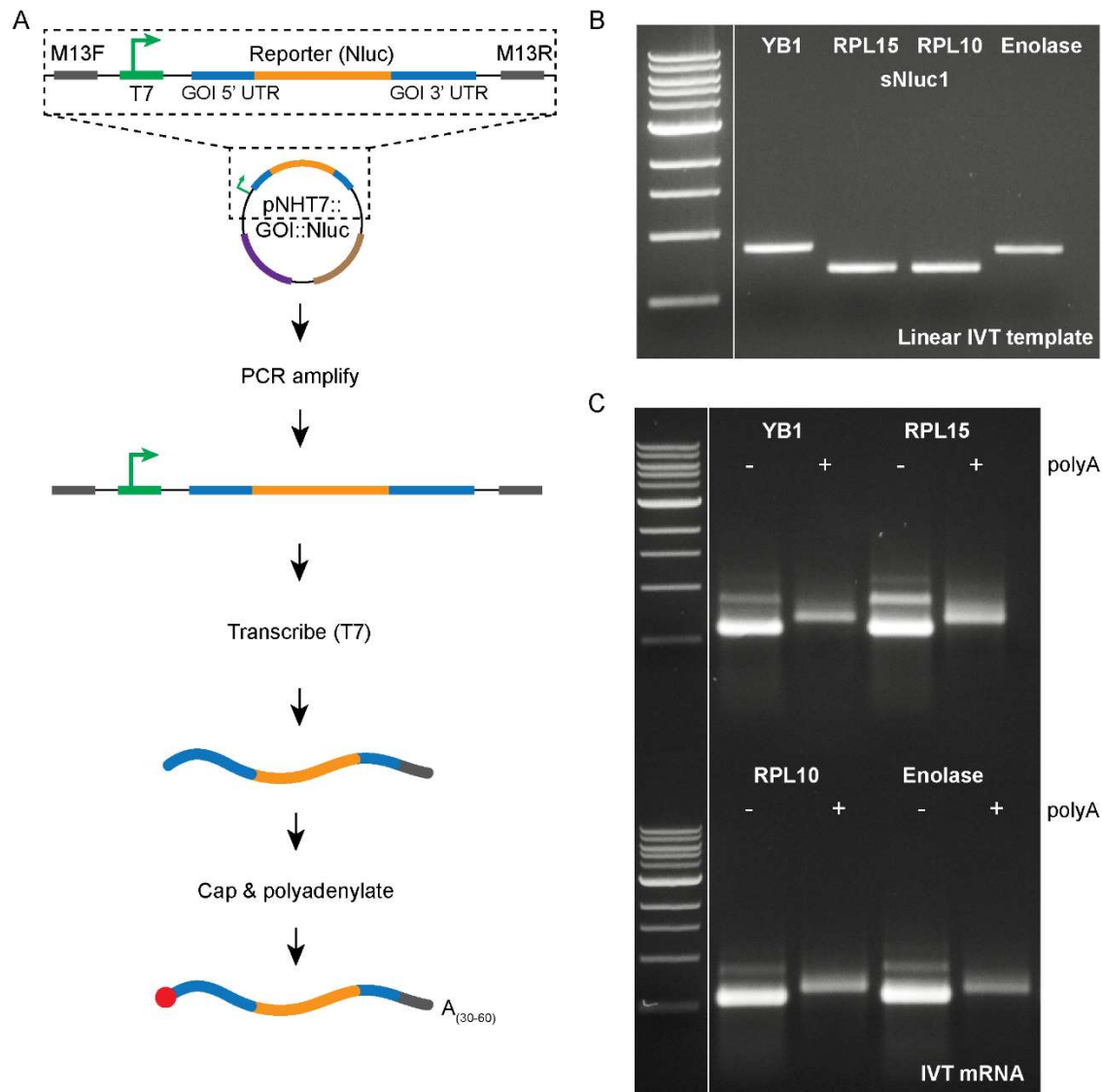
Figure S7: Expected *in vitro* transcription results, related to Figure 3.

(**A**) Diagram of IVT.

(**B**) EtBr stained 1% agarose gel showing the linear amplification products.

(**C**) Gel images showing the mRNA product before and after polyadenylation. Upon successful polyadenylation, the mRNA product should be shifted in size. Samples should be free of excessive degradation products or additional unexpected bands, which we find critical for successful transfections. The ladder used is the NEB 1 kb DNA ladder.

48

994
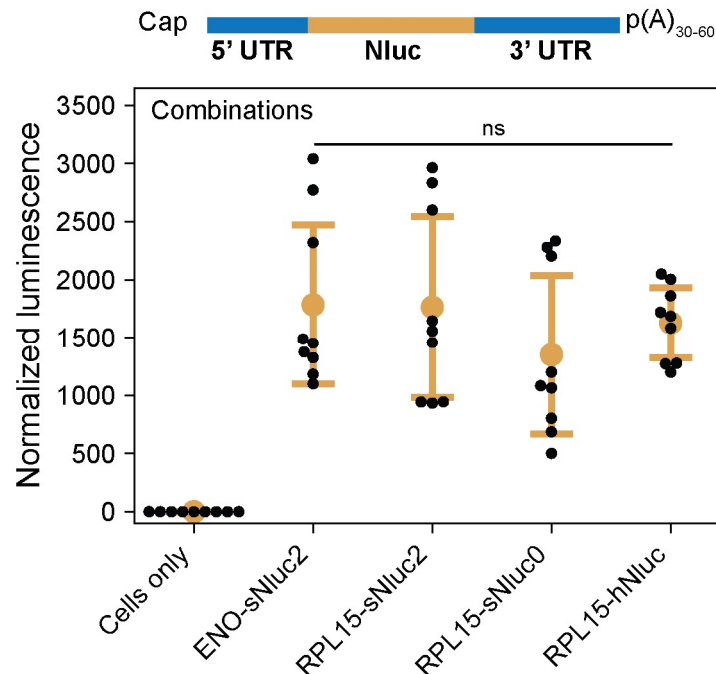
Figure S8: Combinations of UTR sequences with codon optimized Nluc variants, related to Figure 3.

Luminescence from transfections using constructs that combine various UTRs with Nluc codon variants. All transfections are performed with 200,000 cells, from whole dissociated planarians, using 0.8 µL Viromer and 1 µg mRNA per well and assayed 24 hpt.

Statistics. All data points presented are technical replicates (n = 3) from independent biological replicates (n = 3) utilizing mRNA produced from independent IVT reactions. Luminescence measurements are normalized to the mean value of the negative control (cells only). Error bars: standard deviation. Experimental conditions show no statistical significance (ANOVA: p = 0.51).

1004
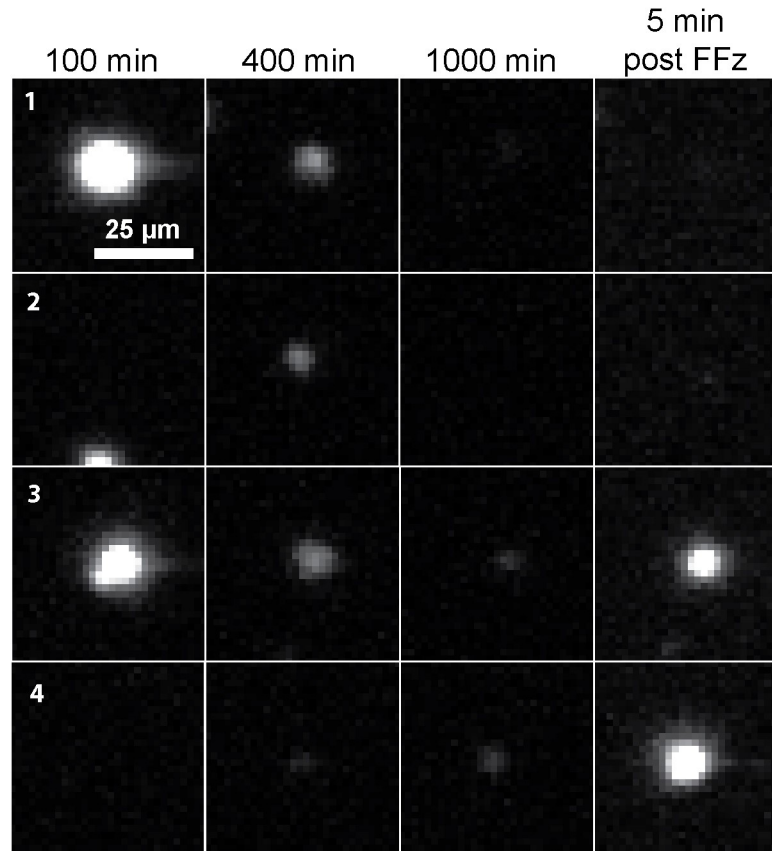
Figure S9. Cell responses to addition of fresh substrate, FFz, after 16 hr of live imaging, related to Figure 4.

200,000 dissociated planarian cells are transfected with 0.8 µL of Viromer and 1 µg of RPL15-sNluc2 mRNA and imaged through a 20× air objective (BoliOptics: BM03023431) at 1 frame per min with a 30 s exposure time for ~17 hr on the custom-built luminescence microscope. After the first imaging session, we add 25 µL of 1:20 FFz diluted in Iso-L15, allow the cells to incubate for 5 min, and acquire an additional post-addition image. Cells exhibit four types of responses. 1. An early-transfected bright cell which does not respond to fresh FFz. 2. A late-transfected dim cell which does not respond to fresh FFz. 3. An early-transfected bright cell which does respond to fresh FFz. 4. A late transfected dim cell which becomes substantially brighter upon addition of fresh FFz.

1016
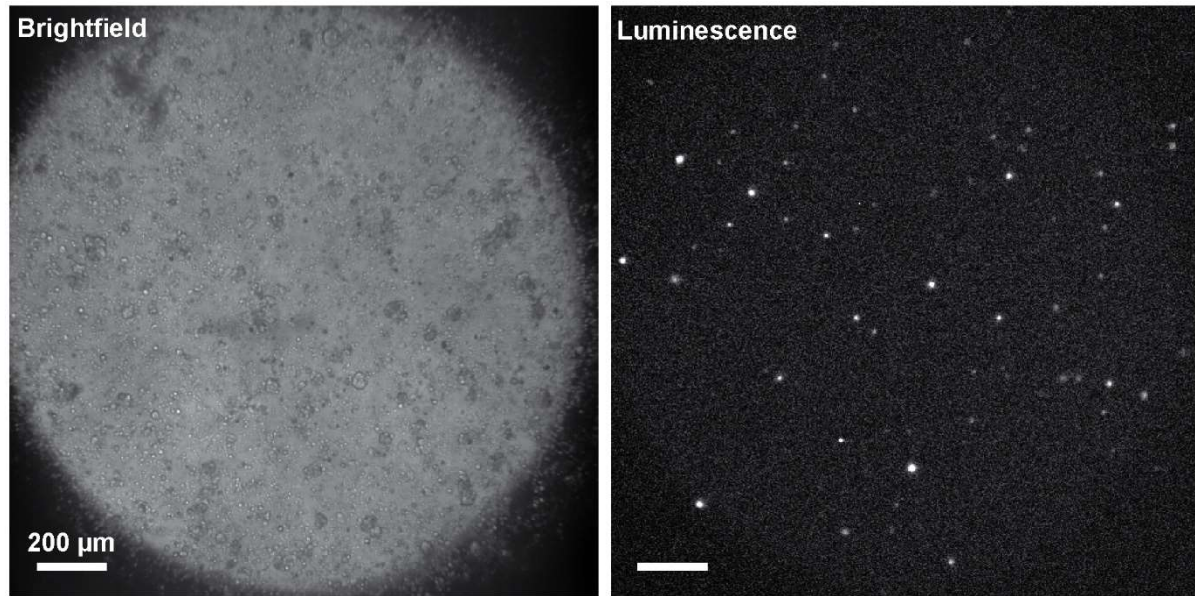
Figure S10: Imaging of dissociated cells after *in vivo* transfection, related to Figure 6.

At 4 hpt using the method described in Figure 6, 10 animals are amputated posterior to the pharynx but anterior to the injection site. The tails are pooled and dissociated, then 1/3 of the cells are plated on a Concanavalin A-treated glass-bottom dish (35 mm). The cells are allowed to settle and adhere for 1 hr, then FFz is added (1:250), and the cells are imaged with a 20× air objective (BoliOptics: BM03023431), with an exposure time of 30 s, and a gain of 500.

1023
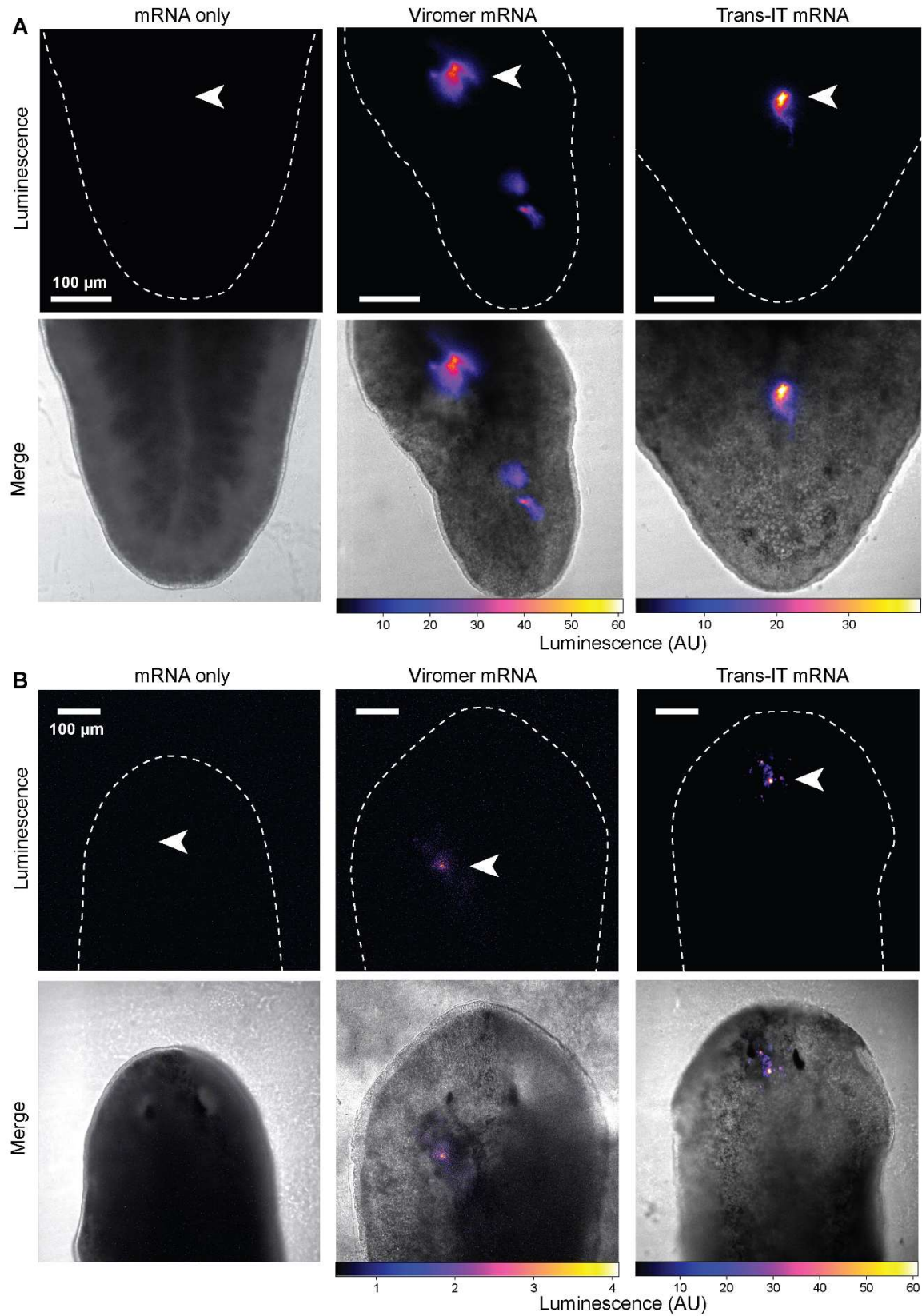
Figure S11: Live imaging of transfected animals, related to Figure 6.

52

1025   (**A**) Planarians injected along the tail midline.

1026   (**B**) Planarians injected at the anterior near the left eye cup. In both experiments live planarians

1027   are imaged on the Olympus LV200 luminescence microscope through a 20× air objective

1028   (Olympus: UPLXAPO20X). Negative control planarians are injected with mRNA alone. Images

1029   are acquired at 12 hpt. Animals are anesthetized and incubated for 15 min in furimazine

1030   (NanoGlo-Live, Promega) supplemented with 1% DMSO to aid in permeabilization.

1031   Luminescence images are acquired using an exposure of 60 s. All experiments are performed

1032   using identical exposure time and digital gain. Transfections are performed according to the

1033   conditions used in **Figure 6B-C**. Dashed lines: tail boundary; arrows: injection sites.
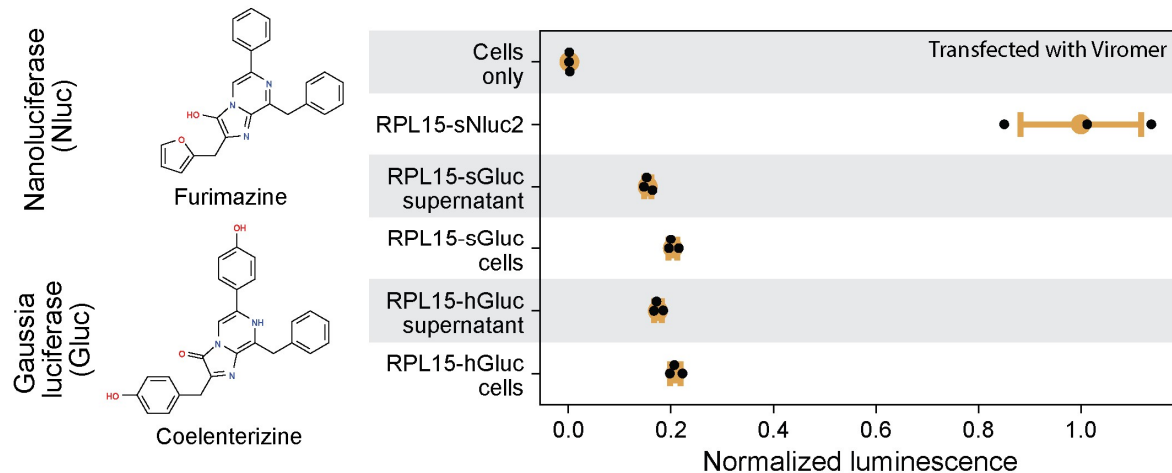
Figure S12: Expression of Gluc in planarian cells.

200,000 bulk dissociated cells are transfected with either RPL15-sGluc (planarian codon optimized), or RPL15-hGluc (human codon optimized) mRNA *in vitro* using Viromer. The cellular pellet and supernatant are separated and assayed independently using the substrate coelenterazine (chemical structure shown on the left) at 24 hpt, as Gluc protein is often secreted (Badr et al., 2007). Indeed, we detect clear signal from both the supernatant and the pellet. Note that luminescence is lower in Gluc transfected cells compared to positive controls transfected with Nluc. Chemical structures of the Nluc and Gluc substrates are shown on the left. All data points represent technical replicates utilizing mRNA prepared from the same batch. Luminescence measurements are normalized to the mean value of RPL15-sNluc2. Error bars, standard deviation.
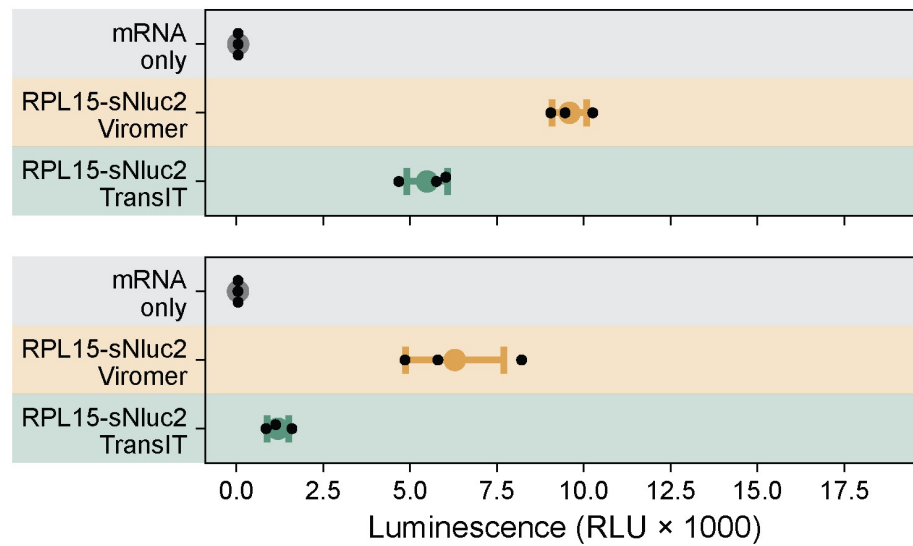
Figure S13: Nluc expression in *Schmidtea polychroa* cells.

Transfections of 200,000 dissociated cells from *S. polychroa* either strain #200 (top) or strain #55 (bottom). Cells are transfected with either 0.8 µL Viromer (yellow) or 2 µL Trans-IT (green) and 1 µg of RPL15-sNluc2 mRNA. Luminescence is assayed 24 hpt. Data points represent technical replicates using mRNA prepared from the same batch. Error bars: standard deviation.

1052
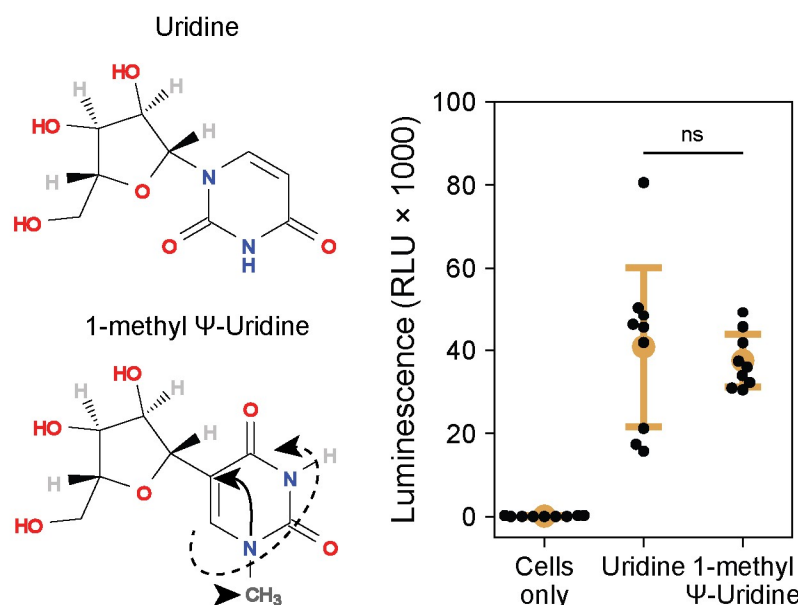
Figure S14: Assessment of m1Ψ on mRNA expression in planarian cells.

Recent reports suggest that the base analog 1-methyl pseudouridine (m1Ψ) may increase translation, improve mRNA stability, and decrease immunogenicity (Andries et al., 2015; Svitkin et al., 2017). This modification is also currently being used in recently developed mRNA vaccines against SARS-CoV-2. We compare transfections with RPL15-sNluc2 mRNA containing either rUTP or m1Ψ (chemical structures shown on the left). We find both to be active, with no significant difference between the two samples (Welch's t-test), suggesting that the observed benefits of m1Ψ modified mRNA in mammalian systems may not be directly transferrable to more basal invertebrates like planarians. Arrow: the uracil group is flipped 180 degrees and attached by a carbon-carbon bond rather than the usual carbon-nitrogen bond in pseudouridine. Arrowhead: m1Ψ contains an additional methyl group. All transfections are conducted with 0.8 μL of Viromer mRNA and 1 μg of mRNA. 200,000 cells are incubated at 20°C, and luminescence is measured at 24 hpt. All data points presented are technical replicates (n = 3) from independent biological replicates (n = 3) utilizing mRNA produced from independent IVT reactions. Error bars: standard deviation.

1068   **Supplemental Tables**

1069

1070   **Table S1: Nluc variants used in this study.** Coding sequences with different codon usage bias

1071   are listed with their respective GC content, and codon adaptation index (CAI) calculated from

1072   https://ppuigbo.me/programs/CAIcal/.

1073

1074   **Table S2: Conditions for screening transfection reagents.** The conditions follow the

1075   manufacturer's protocol. Reagent 1 is the main transfection reagent provided with the kit (e.g.,

1076   Lipofectamine 3000, Trans-IT mRNA, Viromer mRNA). Reagent 2 is a reagent provided by

1077   some but not all kits. For Trans-IT it is the Boost reagent, and for Lipofectamine 3000, it is the

1078   Transfection Enhancer reagent. Diluting Buffer is the solution used to dilute the mRNA and

1079   transfection reagents. Some kits provide a specific buffer to use (Viromer) while others require

1080   serum-free medium, which is L-15 in our experiments. Incubation is done in room temperature

1081   and is recommended to allow the reagent and mRNA to complex before adding to cells.

1082

1083   **Table S3: List of constructs used in this study.** Corresponding plasmid maps are provided in

1084   GenBank (.gb) format as **File S1**. All constructs are available through Addgene.

1085

1086   **Table S4: Primers used in this study.** Listed are primer ID, conventional name, a short

1087   description of the usage, and the sequence from 5' to 3'.

1088   **Supplemental Videos**

1089

1090   **Video S1:** Time-lapse luminescence imaging of RPL15-sNluc2 expressing dissociated planarian

1091   cells immediately after transfection. This video corresponds to the data shown in **Figure 4D-H**.

1092

1093   **Video S2:** Example of luminescent traces for individually segmented cells taken from **Video S1**.

1094

1095   **Video S3:** Montage of luminescence imaging in live planarians, which are decapitated to reduce

1096   motility. This video corresponds to the data shown in **Figure 6E**.

1097

1098   **Video S4:** Live luminescence imaging in planarians immediately post injection. This video

1099   corresponds to the data shown in **Figure 6F-G**.

1100

1101   **Supplemental File**

1102

1103   **File S1:** An archive containing maps for all plasmids (GenBank, .gb) generated and used in this

1104   work.

References

Agata, K., & Watanabe, K. (1999). Molecular and cellular aspects of planarian regeneration. *Seminars in Cell and Developmental Biology*, *10*(4), 377–383. https://doi.org/10.1006/scdb.1999.0324

Aljohani, M. D., El Mouridi, S., Priyadarshini, M., Vargas-Velazquez, A. M., & Frøkjær-Jensen, C. (2020). Engineering rules that minimize germline silencing of transgenes in simple extrachromosomal arrays in C. elegans. *Nature Communications*, *11*(1), 6300. https://doi.org/10.1038/s41467-020-19898-0

Andries, O., Mc Cafferty, S., De Smedt, S. C., Weiss, R., Sanders, N. N., & Kitada, T. (2015). N1-methylpseudouridine-incorporated mRNA outperforms pseudouridine-incorporated mRNA by providing enhanced protein expression and reduced immunogenicity in mammalian cell lines and mice. *Journal of Controlled Release*, *217*(2015), 337–344. https://doi.org/10.1016/j.jconrel.2015.08.051

Badr, C. E., Hewett, J. W., Breakefield, X. O., & Tannous, B. A. (2007). A highly sensitive assay for monitoring the secretory pathway and ER Stress. *PLoS ONE*, *2*(6), e571. https://doi.org/10.1371/journal.pone.0000571

Beal, J., Wagner, T. E., Kitada, T., Azizgolshani, O., Parker, J. M., Densmore, D., & Weiss, R. (2015). Model-driven engineering of gene expression from RNA replicons. *ACS Synthetic Biology*, *4*(1), 48–56. https://doi.org/10.1021/sb500173f

Benazzi, M., Ballester, R., Baguñá, J., & Puccinelli, I. (1972). The fissiparous race of the planarian dugesia lugubris S.L. found in Barcelona (Spain) belongs to the biotype G: Comparative analysis of the karyotypes. *Caryologia*, *25*(1), 59–68. https://doi.org/10.1080/00087114.1972.10796465

Böser, A., Drexler, H. C. A., Reuter, H., Schmitz, H., Wu, G., Schöler, H. R., Gentile, L., & Bartscherer, K. (2013). SILAC Proteomics of Planarians Identifies Ncoa5 as a Conserved Component of Pluripotent Stem Cells. *Cell Reports*, *5*(4), 1142–1155. https://doi.org/10.1016/j.celrep.2013.10.035

Cao, Y., Chen, H., Qiu, R., Hanna, M., Ma, E., Hjort, M., Zhang, A., Lewis, R. S., Wu, J. C., & Melosh, N. A. (2018). Universal intracellular biomolecule delivery with precise dosage control. *Science Advances*, *4*(10), eaat8131. https://doi.org/10.1126/sciadv.aat8131

Cardona, A., Hartenstein, V., & Romero, R. (2006). Early embryogenesis of planaria: A cryptic larva feeding on maternal resources. *Development Genes and Evolution*, *216*(11), 667–681. https://doi.org/10.1007/s00427-006-0094-3

Chen, Z. Y., He, C. Y., Ehrhardt, A., & Kay, M. A. (2003). Minicircle DNA vectors devoid of bacterial DNA result in persistent and high-level transgene expression in vivo. *Molecular Therapy*, *8*(3), 495–500. https://doi.org/10.1016/S1525-0016(03)00168-0

Collins, J. J., Hou, X., Romanova, E. V., Lambrus, B. G., Miller, C. M., Saberi, A., Sweedler, J. V., & Newmark, P. A. (2010). Genome-wide analyses reveal a role for peptide hormones in planarian germline development. *PLoS Biology*, *8*(10), e1000509. https://doi.org/10.1371/journal.pbio.1000509

Davies, E. L., Lei, K., Seidel, C. W., Kroesen, A. E., McKinney, S. A., Guo, L., Robb, S. M. C., Ross, E. J., Gotting, K., & Sánchez Alvarado, A. (2017). Embryonic origin of adult stem cells required for tissue homeostasis and regeneration. *eLife*, *6*, e21052. https://doi.org/10.7554/eLife.21052

Edelstein, A. D., Tsuchida, M. A., Amodaj, N., Pinkard, H., Vale, R. D., & Stuurman, N. (2014). Advanced methods of microscope control using μManager software. Journal of Biological

1151   Methods, 1(2), e10. https://doi.org/10.14440/jbm.2014.36

1152 England, C. G., Ehlerding, E. B., & Cai, W. (2016). NanoLuc: A small luciferase is brightening
1153   up the field of bioluminescence. *Bioconjugate Chemistry*, *27*(5), 1175–1187.
1154   https://doi.org/10.1021/acs.bioconjchem.6b00112

1155 Fincher, C. T., Wurtzel, O., de Hoog, T., Kravarik, K. M., & Reddien, P. W. (2018). Cell type
1156   transcriptome atlas for the planarian *Schmidtea mediterranea*. *Science*, *360*(6391),
1157   eaaq1736. https://doi.org/10.1126/science.aaq1736

1158 González-Estévez, C., Momose, T., Gehring, W. J., & Saló, E. (2003). Transgenic planarian lines
1159   obtained by electroporation using transposon-derived vectors and an eye-specific GFP
1160   marker. *Proceedings of the National Academy of Sciences of the United States of America*,
1161   *100*(24), 14046–14051. https://doi.org/10.1073/pnas.2335980100

1162 Grohme, M. A., Schloissnig, S., Rozanski, A., Pippel, M., Young, G. R., Winkler, S., Brandl, H.,
1163   Henry, I., Dahl, A., Powell, S., Hiller, M., Myers, E., & Rink, J. C. (2018). The genome of
1164   *Schmidtea mediterranea* and the evolution of core cellular mechanisms. *Nature*, *554*(7690),
1165   56–61. https://doi.org/10.1038/nature25473

1166 Guo, L., Bloom, J., Dols Serrate, D., Boocock, J., Ben David, E., Schubert, O. T., Kazuma, K.,
1167   Ho, K., Warda, E., Chui, C., Wei, Y., Leighton, D., Lemus Vergara, T., Riutort, M.,
1168   Sánchez Alvarado, A., & Kruglyak, L. (2022). Island-specific evolution of a sex-primed
1169   autosome in the planarian. *Nature*, https://doi.org/10.1038/s41586-022-04757-3

1170 Guo, L., Zhang, S., Rubinstein, B., Ross, E., & Sánchez Alvarado, A. (2017). Widespread
1171   maintenance of genome heterozygosity in *Schmidtea mediterranea*. *Nature Ecology &*
1172   *Evolution*, *1*(1), 19. https://doi.org/10.1038/s41559-016-0019

1173 Hall, M. P., Unch, J., Binkowski, B. F., Valley, M. P., Butler, B. L., Wood, M. G., Otto, P.,
1174   Zimmerman, K., Vidugiris, G., MacHleidt, T., Robers, M. B., Benink, H. A., Eggers, C. T.,
1175   Slater, M. R., Meisenheimer, P. L., Klaubert, D. H., Fan, F., Encell, L. P., & Wood, K. V.
1176   (2012). Engineered luciferase reporter from a deep sea shrimp utilizing a novel
1177   imidazopyrazinone substrate. *ACS Chemical Biology*, *7*(11), 1848–1857.
1178   https://doi.org/10.1021/cb3002478

1179 Hayashi, T., Asami, M., Higuchi, S., Shibata, N., & Agata, K. (2006). Isolation of planarian X-
1180   ray-sensitive stem cells by fluorescence-activated cell sorting. *Development Growth and*
1181   *Differentiation*, *48*(6), 371–380. https://doi.org/10.1111/j.1440-169X.2006.00876.x

1182 Jeacock, L., Faria, J., & Horn, D. (2018). Codon usage bias controls mRNA and protein
1183   abundance in trypanosomatids. *eLife*, *7*, e32496. https://doi.org/10.7554/eLife.32496

1184 Kim, T. J., Türkcan, S., & Pratx, G. (2017). Modular low-light microscope for imaging cellular
1185   bioluminescence and radioluminescence. *Nature Protocols*, *12*(5), 1055–1076.
1186   https://doi.org/10.1038/nprot.2017.008

1187 Kim, I. V., Duncan, E. M., Ross, E. J., Gorbovytska, V., Nowotarski, S. H., Elliott, S. A.,
1188   Sánchez Alvarado, A., & Kuhn, C. D. (2019). Planarians recruit piRNAs for mRNA
1189   turnover in adult stem cells. *Genes & Development*, *33*(21–22), 1575–1590.
1190   https://doi.org/10.1101/gad.322776.118

1191 Lakshmanan, V., Bansai, D., Kulkarni, J., Poduval, D., Krishna, S., Sasidharan, V., Anand, P.,
1192   Seshasayee, A., & Palakodeti, D. (2016). Genome-wide analysis of polyadenylation events
1193   in *Schmidtea mediterranea*. *G3: Genes, Genomes, Genetics*, *6*(10), 3035–3048.
1194   https://doi.org/10.1534/g3.116.031120

1195 Lei, K., McKinney, S. A., Ross, E. J., Lee, H. C., & Sánchez Alvarado, A. (2019). Cultured
1196   pluripotent planarian stem cells retain potency and express proteins from exogenously

1197   introduced mRNAs. *BioRxiv*, 573725. https://doi.org/10.1101/573725

1198   Leonhardt, C., Schwake, G., Stögbauer, T. R., Rappl, S., Kuhr, J. T., Ligon, T. S., & Rädler, J.
1199   O. (2014). Single-cell mRNA transfection studies: Delivery, kinetics and statistics by
1200   numbers. *Nanomedicine: Nanotechnology, Biology, and Medicine*, *10*(4), 679–688.
1201   https://doi.org/10.1016/j.nano.2013.11.008

1202   Leppek, K., Byeon, G. W., Kladwang, W., Wayment-Steele, H. K., Kerr, C. H., Xu, A. F., Kim,
1203   D. S., Topkar, V. V., Choe, C., Rothschild, D., Tiu, G. C., Wellington-Oguri, R., Fujii, K.,
1204   Sharma, E., Watkins, A. M., Nicol, J. J., Romano, J., Tunguz, B., Diaz, F., … Das, R.
1205   (2022). Combinatorial optimization of mRNA structure, stability, and translation for RNA-
1206   based therapeutics. *Nature Communications*, *13*(1), 1536. https://doi.org/10.1038/s41467-
1207   022-28776-w

1208   Lim, Y., Shiver, A. L., Khariton, M., Lane, K. M., Ng, K. M., Bray, S. R., Qin, J., Huang, K. C.,
1209   & Wang, B. (2019). Mechanically resolved imaging of bacteria using expansion
1210   microscopy. *PLOS Biology*, *17*(10), e3000268.
1211   https://doi.org/10.1371/journal.pbio.3000268

1212   Lostalé-Seijo, I., & Montenegro, J. (2018). Synthetic materials at the forefront of gene delivery.
1213   *Nature Reviews Chemistry 2*(10), 258–277. https://doi.org/10.1038/s41570-018-0039-1

1214   Newmark, P. A., & Sánchez Alvarado, A. (2002). Not your father's planarian: A classic model
1215   enters the era of functional genomics. *Nature Reviews Genetics*, *3*(3), 210–219.
1216   https://doi.org/10.1038/nrg759

1217   Plass, M., Solana, J., Wolf, F. A., Ayoub, S., Misios, A., Glažar, P., Obermayer, B., Theis, F.J.,
1218   Kocks, C., & Rajewsky, N. (2018). Cell type atlas and lineage tree of a whole complex
1219   animal by single-cell transcriptomics. *Science*, *360*(6391), eaaq1723. DOI:
1220   10.1126/science.aaq1723

1221   Puigbò, P., Bravo, I. G., & Garcia-Vallve, S. (2008). CAIcal: A combined set of tools to assess
1222   codon usage adaptation. *Biology Direct*, *3*(1), 38. https://doi.org/10.1186/1745-6150-3-38

1223   Quax, T. E. F., Claassens, N. J., Söll, D., & van der Oost, J. (2015). Codon bias as a means to
1224   fine-tune gene expression. *Molecular Cell*, *59*(2), 149–161.
1225   https://doi.org/10.1016/j.molcel.2015.05.035

1226   Raz, A. A., Wurtzel, O., & Reddien, P. W. (2021). Planarian stem cells specify fate yet retain
1227   potency during the cell cycle. *Cell Stem Cell*, *28*(7), 1307-1322.
1228   https://doi.org/10.1016/j.stem.2021.03.021

1229   Reddien, P. W. (2018). The cellular and molecular basis for planarian regeneration. *Cell*, *175*(2),
1230   327–345. https://doi.org/10.1016/j.cell.2018.09.021

1231   Reddien, P. W., Bermange, A. L., Murfitt, K. J., Jennings, J. R., & Sánchez Alvarado, A. (2005).
1232   Identification of genes needed for regeneration, stem cell function, and tissue homeostasis
1233   by systematic gene perturbation in planaria. *Developmental Cell*, *8*(5), 635–649.
1234   https://doi.org/10.1016/j.devcel.2005.02.014

1235   Rink, J. C. (2018). Stem cells, patterning and regeneration in planarians: Self-organization at the
1236   organismal scale. In *Methods in Molecular Biology*, *1774*, 57–172.
1237   https://doi.org/10.1007/978-1-4939-7802-1_2

1238   Rossi, A., Ross, E. J., Jack, A., & Sánchez Alvarado, A. (2014). Molecular cloning and
1239   characterization of SL3: A stem cell-specific SL RNA from the planarian *Schmidtea*
1240   *mediterranea*. *Gene*, *533*(1), 156–167. https://doi.org/10.1016/j.gene.2013.09.101

1241   Rozanski, A., Moon, H. K., Brandl, H., Martín-Durán, J. M., Grohme, M. A., Hüttner, K.,
1242   Bartscherer, K., Henry, I., & Rink, J. C. (2019). PlanMine 3.0 - improvements to a mineable

1243   resource of flatworm biology and biodiversity. *Nucleic Acids Research*, *47*(D1), D812–
1244   D820. https://doi.org/10.1093/nar/gky1070
1245 Sánchez Alvarado, A., & Newmark, P. A. (1999). Double-stranded RNA specifically disrupts
1246   gene expression during planarian regeneration. *Proceedings of the National Academy of
1247   Sciences of the United States of America*, *96*(9), 5049–5054.
1248   https://doi.org/10.1073/pnas.96.9.5049
1249 Schindelin, J., Arganda-Carreras, I., Frise, E., Kaynig, V., Longair, M., Pietzsch, T., Preibisch,
1250   S., Rueden, C., Saalfeld, S., Schmid, B., Tinevez, J. Y., White, D. J., Hartenstein, V.,
1251   Eliceiri, K., Tomancak, P., & Cardona, A. (2012). Fiji: An open-source platform for
1252   biological-image analysis. *Nature Methods*, *9*(7), 676–682.
1253   https://doi.org/10.1038/nmeth.2019
1254 Schmiderer, L., Subramaniam, A., Žemaitis, K., Bäckström, A., Yudovich, D., Soboleva, S.,
1255   Galeev, R., Prinz, C. N., Larsson, J., & Hjort, M. (2020). Efficient and nontoxic
1256   biomolecule delivery to primary human hematopoietic stem cells using nanostraws.
1257   *Proceedings of the National Academy of Sciences of the United States of America*, *117*(35),
1258   21267–21273. https://doi.org/10.1073/pnas.2001367117
1259 Sharp, P. M., & Li, W. H. (1987). The codon adaptation index-a measure of directional
1260   synonymous codon usage bias, and its potential applications. *Nucleic Acids Research*,
1261   *15*(3), 1281–1295. https://doi.org/10.1093/nar/15.3.1281
1262 Su, Y., Walker, J. R., Park, Y., Smith, T. P., Liu, L. X., Hall, M. P., Labanieh, L., Hurst, R.,
1263   Wang, D. C., Encell, L. P., Kim, N., Zhang, F., Kay, M. A., Casey, K. M., Majzner, R. G.,
1264   Cochran, J. R., Mackall, C. L., Kirkland, T. A., & Lin, M. Z. (2020). Novel NanoLuc
1265   substrates enable bright two-population bioluminescence imaging in animals. *Nature
1266   Methods*, *17*(8), 852–860. https://doi.org/10.1038/s41592-020-0889-6
1267 Svitkin, Y. V., Cheng, Y. M., Chakraborty, T., Presnyak, V., John, M., & Sonenberg, N. (2017).
1268   N1-methyl-pseudouridine in mRNA enhances translation through eIF2α-dependent and
1269   independent mechanisms by increasing ribosome density. *Nucleic Acids Research*, *45*(10),
1270   6023–6036. https://doi.org/10.1093/nar/gkx135
1271 Taning, C. N. T., Christiaens, O., Li, X., Swevers, L., Casteels, H., Maes, M., & Smagghe, G.
1272   (2018). Engineered flock house virus for targeted gene suppression through RNAi in fruit
1273   flies (*Drosophila melanogaster*) *in vitro* and *in vivo*. *Frontiers in Physiology*, *9*(805), 1–13.
1274   https://doi.org/10.3389/fphys.2018.00805
1275 Tay, A., & Melosh, N. (2019). Transfection with nanostructure electro-injection is minimally
1276   perturbative. *Advanced Therapeutics*, *2*(12), 1900133.
1277   https://doi.org/10.1002/adtp.201900133
1278 van der Walt, S., Schönberger, J. L., Nunez-Iglesias, J., Boulogne, F., Warner, J. D., Yager, N.,
1279   Gouillart, E., & Yu, T. (2014). Scikit-image: Image processing in python. *PeerJ*, *2*:e453.
1280   https://doi.org/10.7717/peerj.453
1281 Vila-Farré, M., & Rink, J. C. (2018). The ecology of freshwater planarians. In *Methods in
1282   Molecular Biology*, *1774*, 173–205. https://doi.org/10.1007/978-1-4939-7802-1_3
1283 Wagner, D. E., Wang, I. E., & Reddien, P. W. (2011). Clonogenic neoblasts are pluripotent adult
1284   stem cells that underlie planarian regeneration. *Science*, *332*(6031), 811–816.
1285   https://doi.org/10.1126/science.1203983
1286 Xie, X., Xu, A. M., Leal-Ortiz, S., Cao, Y., Garner, C. C., & Melosh, N. A. (2013). Nanostraw-
1287   electroporation system for highly efficient intracellular delivery and transfection. *ACS
1288   Nano*, *7*(5), 4351–4358. https://doi.org/10.1021/nn400874a

1289   Zayas, R. M., Bold, T. D., & Newmark, P. A. (2005). Spliced-leader trans-splicing in freshwater
1290   planarians. *Molecular Biology and Evolution*, *22*(10), 2048–2054.
1291   https://doi.org/10.1093/molbev/msi200